MASTERARBEIT / MASTER'S THESIS

Titel der Masterarbeit / Title of the Master's Thesis

„Investigation of nuclear mechanics and coherent dynamics in relation to the changing local chemical environment“

verfasst von / submitted by

Elena Kirilova Chayleva

angestrebter akademischer Grad / in partial fulfilment of the requirements for the degree of

Master of Science (MSc)

Wien, 2023 / Vienna, 2023

Studienkennzahl lt. Studienblatt / degree programme code as it appears on the student record sheet:	UA 066877
Studienrichtung lt. Studienblatt / degree programme as it appears on the student record sheet:	Masterstudium Genetik und Entwicklungsbiologie
Betreut von / Supervisor:	Assoz. Prof. Dipl.-Ing. Dr. Thomas Juffmann

Table of Contents

Acknowledgement

I would like to express my deep appreciation to Professor Thomas Juffmann, who agreed to become my master's thesis supervisor.

The process was carried out at the Medical University of Vienna under the direct leadership of Dr. Kareem Elsayad. Words cannot describe the gratitude and respect I have for him. At the very beginning, he showed me the biophysics lab and explained to me both the mechanism of working with the Brillouin microscope and a bit about the history and development of applications to date. My training started with searching for information on topics concerning biomechanics and biophysics, dynamics in the nucleus, and how ion concentrations can be measured in different ways. Eventually, I learned about the MatLab program, which is used to run the analyses. The laboratory exercises started with learning the methodology of working with the microscope and getting a clear picture. In the beginning, I measured water, mineral oil, and glue. The process was long and difficult. We drew up a timetable for the different stages and allocated them in the time we were given. There were times when I even wanted to give up, feeling frustrated in this new field. However, Dr. Elsayad stepped in and helped me, giving me advice and guidance not only on the specific problem but also on how to reason. I began to understand the subject, the meaning of the research, and the real-life applications better and better. Regarding the computer program, I have studied what has been written so far about close analysis, did research, and watched videos. However, I felt a lack of knowledge, and I did not want to consult my mentor at every minor setback. I enrolled in two courses at an online academy that increased my knowledge. Since we already had enough results from various analyses with Dr. Elsayad, we decided to start writing a thesis so that it could be gradual and at least partially reduce the stress of the demanding process. We discussed the structure of the master's thesis and the subparts it would contain. To perform better and make the examiner's job easier, I enrolled in an online course on research paper writing at Stanford University. I worked hard in all directions, from measurements to analyses to describing results. During my 6-month stay, I was privileged to be part of the team that published a paper on in situ applications of the Brillouin microscope in medicine, as well as to participate in the MIC conference of the Medical University of Vienna. Again, the opportunities were provided by my direct advisor.

I deeply appreciate the help, guidance, and chances. You took a risk by choosing a genetics Master student who came to this country a year ago for such a high level in biophysics, and I will not forget it. I hope we will have the opportunity to work together in the future.

I could not miss to express my gratitude to Professor Christian Schöfer who prepared the HeLa cells for the research and subsequently agreed to be my examiner during the defence.

I would also like to acknowledge Dr. Ivan Yudushkin, who mentioned me for this position and helped me with all documents, according to registration and thesis submission.

Without all of you, this master's thesis would not be a reality, and I may never have had the honor of taking and defending a master's degree in genetics and molecular pathology. You have shown me that my dream can be realized.

Abstract

Mechanical properties across different scales are essential for establishing the necessary organization and structure for biological cells to function, with changes therein associated with diverse pathologies. Measuring the relevant mechanical properties is however far from trivial. Through a new generation of micro-spectroscopy approaches based on Brillouin light scattering, it has become possible to non-invasively measure the microscopic high-frequency elastic and viscous properties with a high spatial and temporal resolution. Key advantages of this technology are that it is all-optical, label-free, non-invasive and non-perturbative. A major challenge however is the interpretation and significance of the mechanical properties measured with Brillouin spectroscopy, which are associated with distinct spatial-temporal scales and boundary conditions to those of more common mechanical measurement techniques. For one these mechanical parameters are known to be acutely sensitive to the phase state and the degree and nature of hydration. The focus of this Master thesis is twofold: 1. Exploring the potential of this technology for differentiation of tissues in situ towards clinical/medical applications. 2. Exploring the dynamic mechanical properties of living cell nuclei and how these are affected by different perturbations.

Zusammenfassung

Mechanische Eigenschaften in verschiedenen Größenordnungen sind von wesentlicher Bedeutung für die Organisation und Struktur, die biologische Zellen für ihr Funktionieren benötigen, und Veränderungen dieser Eigenschaften sind bekanntlich mit verschiedenen Krankheiten verbunden. Die Messung der relevanten mechanischen Eigenschaften ist jedoch alles andere als trivial. Durch eine neue Generation von Mikro Spektroskopieansätzen, die auf Brillouin-Lichtstreuung basieren, ist es möglich geworden, die mikroskopischen hochfrequenten elastischen und viskosen Eigenschaften mit einer hohen räumlichen und zeitlichen Auflösung nicht-invasiv zu messen. Die Hauptvorteile dieser Technologie sind, dass sie rein optisch, markierungsfrei, nicht-invasiv und nicht-störend ist. Eine große Herausforderung ist jedoch die Interpretation und Aussagekraft der mit der Brillouin-Spektroskopie gemessenen mechanischen Eigenschaften, die mit anderen räumlich-zeitlichen Skalen und Randbedingungen verbunden sind als bei den üblichen mechanischen Messverfahren. Zum einen ist bekannt, dass diese mechanischen Parameter sehr empfindlich auf den Phasenzustand sowie den Grad und die Art der Hydratation reagieren. Diese Masterarbeit hat zwei Schwerpunkte: 1. die Erforschung des Potenzials dieser Technologie für die Differenzierung von Geweben in situ für klinische/medizinische Anwendungen. 2. Erforschung der dynamischen mechanischen und Phaseneigenschaften von lebenden Zellkernen und deren Beeinflussung durch verschiedene Störeinflüsse.

Chapter 1. Introduction

1.1. Importance of mechanical properties in Biology

Biomechanics concerns the study of the mechanical principles and properties of living organisms, in relation to their movement and structure (Oxford English Dictionary, 2010). As part of biophysics it includes the study on the level of organisms, cells, and organelles. To exist and function, these must all possess tightly regulated characteristics such as mechanical strength, flexibility, and compressive and tensile strength. In living cells, these also often need to be dynamic and tuneable on different spatial and temporal scales. Biomechanics is used to analyse and understand human movement patterns, such as walking, running, jumping, and throwing. This includes studying joint kinematics (movement) and kinetics (forces) to determine how forces are generated, distributed, and controlled within the body during different activities. The mechanical properties of muscles for example, are important indicators of their functionality, and deviations from optimum properties can be indicative of various diseases (19, 43, 51) and help in the realization of better rehabilitation strategies, monitor progress during recovery. The mechanical properties are also important for developing optimum prosthetics, orthotics, and implants. The mechanical compatibility between implantable devices and biological tissues is essential for their long-term performance and biocompatibility. This extends to other tissue,with diseases as diverse as Alzheimers, cancer, artherosclerosis, cardiac diseases, and diabetes all associated with changes in the mechanical properties of the affected tissues. Measuring these non-invasively is from a surgical and diagnostic perspective highly desirable.

On the microscopic scale, cell stiffness, adhesion, and deformability influence processes such as cell migration, tissue development, and immune response. These are directly related to processes on larger scale such as organ function, with variations in the single cells and organelle structures and mechanics associated with various diseases (43, 51).

1.2. How do we measure mechanical properties in Biology

Mechanical testing of bulk specimens by simple deformations in different directions is one of the oldest methods for extracting the elastic properties. Applying this in different directions sequentially can be used to explain the three-dimensional shape and structure (1). The stiffness coefficients can be calculated using a generalized Hooke's Law: $\varepsilon i = Sij\sigma ji, j,i = 1$ to 6, where epsilon is the applied stress, sigma is the resulting strain, and Sij the compliance

(inverse of the stiffness) (2). A major downside of this approach is that it requires physical access to the region of interest. As such the studied region needs to either be on the surface or isolated. Finally, it is also by design perturbative which may prove limiting for sensitive samples. One extension of this is Atomic force microscopy, which measures the forces in cells and molecules. The structure includes a silicon conical probe that pokes the sample. The result is an arm deflection, which in turn is measured by the reflection of a laser signal. The biggest advantage is the resolution can be as small as 1 nm and one can map a sample in 2D. When measuring live cells, an optical microscope is used to precisely place the probe on the sample to be examined. A significant drawback is that the probe tip often applies significant forces to the cell (4) that may affect the cell in question, and that one is limited to the surface.

Another commonly used technique is resonant ultrasound spectroscopy. It is based on the appearance of unique vibrational frequencies in an excited state. The system consists of two piezoelectric transducers, with the sample in between. The first one emits a variable frequency and the second one finds the resonance of the cell. The principle is based on the fact that acoustic properties are directly related to the mechanical properties, in other words, that the mechanical properties will affect the propagation characteristics of an acoustic field. As such it becomes possible to extract the stiffness. The method is fast and accurate (3), however has the disadvantage that it depends on the sample size and shape, and unsuitable for clinical applications.

For measuring the mechanics on the nanoscopic scale optical tweezers can be used. Here a small bead is coated with fibronectin and bound to the target sample. A beam of light is focused (optically trapping the bead) and moves laterally, tracking the movement of the bead. The process is based on the principle of creating an optical trap with which one can apply a small controlled force (4). Knowing this force and the resulting displacement of the bead allows one to calculate an elastic modulus using Hooke's law (see above). The advantage is that one obtains information at the molecular level. On the other hand, the beam strength affects the measurement and can lead to the phototoxicity of the cell, and it is by design unsuitable for mapping the mechanics spatially or being applied in a clinical setting.

There are numerous other techniques for measuring mechanical properties including passive microrheology (9, 22, 40), optical coherence elastography (22, 48, 49, 58), and micropipette asperation (for cells) (11) and traction force microscopy (6, 31, 33). A common theme is that

these either are not capable of spatial mapping properties inside living cells, require the physical perturbation of a sample, or require specific labels to be introduced into the sample.

1.3. Brillouin scattering

The Brillouin scattering microscopy offers a means on non-contact label-free measurement of the elastic and viscous properties at a specific point on an object using light. It was first described in 1922 by Brillouin as a coherent beam emerging from scattered acoustic waves that undergoes a frequency variation equal to that of the acoustic wave. A few years later this was confirmed by Gross (2, 3). The scattering waves could include phonons (inherent or stimulated acoustic modes) as well as magnons/spin waves. For biological samples only the former are relevant. The propagating acoustic (density) wave mean that there is a change in frequency of the reflected light because of the Doppler effect. In weak elastic attenuation, the elastic scattering has the most intense signal, while the Brillouin scattering is contained in two peaks (a Stoke and an anti-Stokes) equally distant from the elastic peak. The frequency of these can be calculated by the formula $\omega B = \pm Vq$, where the Brillouin signal is represented as the product of the acoustic wave speed (V) and the wavevector (q) in the scattering process. The latter depends on the index of refraction, the angle of scattering, and the incident light: $q = \frac{nki2sin\theta}{2}$, where ki is 2*pi/lambda, and lambda is the free space probing wavelength. The elasticity (longitudinal modulus) can be calculated as $M = \rho V^2 = \rho \frac{\omega B^2}{q2} = \frac{q\omega B^2}{n^2 4k_i^2}$.

The longitudinal modulus is the sum of the bulk modulus (K) and that of the shear modulus (G): $M = K + (4/3)G$.

As mentioned above, mechanical properties depend both on the probed spatial and time scales. In Brillouin spectroscopy the spatial scales are those of the phonons, which are a few hundred nanometres (smaller than diffraction limit). The time scales are also those of the phonons which are picoseconds to nanoseconds since the probed phonons are in the GHz energy range. These are very fast time scales, not usually probed with any of the above mentioned techniques (the closes being ultrasounds, which is in the kHz-MHz range). To appreciate the relevant time-scales we show the frequency dispersion of the longitudinal modulus for a solid, gel and liquid in *Figure 1* (5). Here the shaded region shows the GHz range.

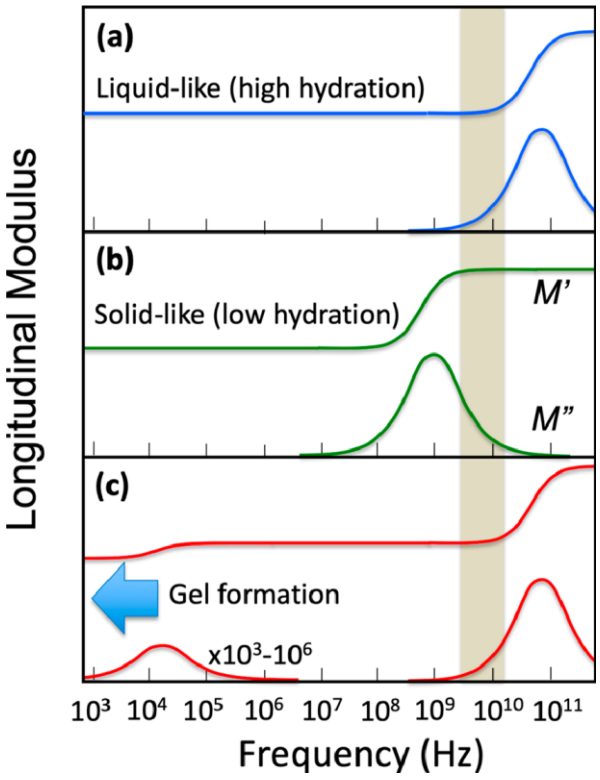

Figure 1 Typical dispersion curves relative to the longitudinal elastic modulus of samples with a structural relaxation rate (a) higher (liquidlike) and (b) lower (solid-like) than the Brillouin peak, usually falling within the shadowed region of the plot. The case (c) refers to a heterogeneous sample, where a small fraction of arrested state is forming within a large fraction of liquid sample, giving rise to a gel phase. Taken from Ref (5)

In each case the top plot shows the storage modulus while the bottom shows the loss modulus. In *1A* BLS measures a viscoelasticity very similar to that at lower frequencies, since it is still far below the liquid relaxation times (which are at >THz) and there are no slower relaxation processes. *Fig 1B* shows the case of a solid. Here there are slower relaxation processes due to the solid state (proteins for example will have relaxation times on the order of kHz), that will cause a larger storage modulus also at the GHz frequencies. Finally in *1C* a gel-like state is shown that has both slower and the fast liquid relaxation. From this it can be appreciated that: (1) BLS can be very sensitive to the phase state and to study phase transitions. (2) By studying also the loss properties (via the BLS linewidth) one can estimate the relaxation times of the system which can tell one of its content and the nature of molecular interactions. (3) The properties measured in BLS, while potentially serving as a useful proxy to the "everyday macroscopic" mechanics measure a fundamentally different regime than the techniques described above, and the extracted values cannot be directly inserted into such models.

The advantages of the Brillouin microscope examination are non-contact, fast signal generation, and measurement of biological samples with micro dimensions. Non-homogeneous heterogeneous samples are visualized in a dynamic state. This allows for real-time information on temporal and spatial variation. It is applicable in various scientific fields: physics, biology, cell culture, and engineering (2, 15, 36).

Challenges in the Brillouin measurement can come from the high laser power and the illumination dose often used, which can lead to the phototoxicity of cells. In our measurements, using the latest generation of BLS spectrometers, we are careful to keep laser intensity and exposure below such levels.

An example of the type of potentially useful information that can be extracted from BLS is shown in *Figure 2*. Shown here is that different brain regions are associated with quite different elastic moduli (8). This is interesting insofar that lower elasticity is known to be linked to injuries and activates pathology (8, 40).

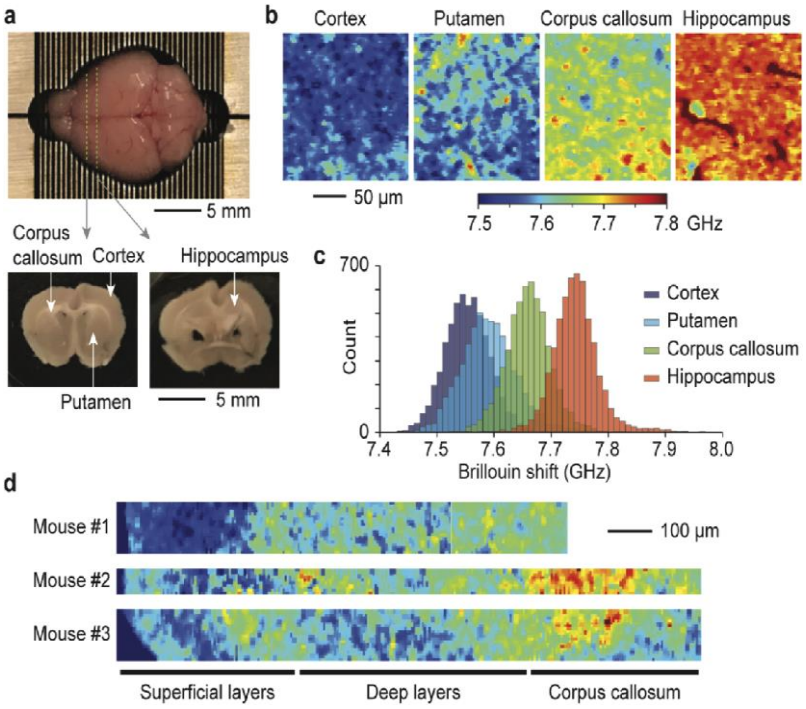

Figure 2 Brillouin images of brain tissue slices. a, Coronal brain slices obtained from a 6-week old female mouse at -1 and -2 mm from the bregma. b, Brillouin images taken at a depth of 50 µm from the tissue surface at four anatomically distinct sites: cortex, putamen, corpus callosum, and hippocampus. c, Histogram of Brillouin shifts in the four different regions. d, Brillouin maps of brain tissue slices from three different mice taken across the sub-cortical layers and corpus callosum. Taken from Ref (8)

1.4. Summary of thesis

The graduation thesis, "Investigating nuclear mechanics and coherent dynamics in relation to the changing local chemical environment", is composed of four chapters, each of them dealing with a different aspect of biophysics. Chapter 1 is introductory and defines the mechanical properties of Biology. It is subdivided into three parts. Part 1 describes the importance of mechanical properties in Biology and explains fundamental principles, their meaning, and how we can measure the mechanics in cells. Then, it deals with Brillouin scattering, what it is based on, its applications, and its limitations. Also, it illustrates what it has already been used for in Biology.

Chapter 2 examines the anatomy part. It consists of six subdivisions. The first one focuses on the physiological processes and proper functioning of internal systems, in addition to measuring the viscoelastic properties of bone, muscle tissue, and blood vessels. Parts 2–6 provide an outline of the relevant state of the art, experiments, results, and discussion. At the end, the conclusion and importance of experiments. The mechanics can exceed our knowledge in diseases and health.

Chapter 3 concentrates on problems resulting from perturbations on the nucleus that come from different PBS concentrations, as well as incompatible temperatures. The skeleton bone followed the same structure. We understand now better the nuclear mechanics and how cells replicated, also the control of genetic information.

General conclusions, outlook and future perspectives are drawn in Chapter 4. The main aim of the graduation thesis has been reached. It includes some suggestions on how we should go forward.

Chapter 2: 2.1. Anatomy part

A large part of biomechanics is related to the anatomy of living organisms. Measuring the viscoelastic properties of bone, muscle tissue, and blood vessels gives us information about their health and function. Non-contact measurements using Brillouin microscopy can reveal information on their elastic modulus and viscosity.

In terms of clinical diagnosis, this provides the potential to detect pathological abnormalities using a minimally invasive method. An biopsy of <1 cm of tissue is sufficient to perform such measurements. The method can potentially be applied on living persons, we here however only test on donor samples. It has potential drawbacks such as phototoxicity at high laser intensity, required alignment of the system before use, evaluation of controls each time, and specific knowledge of microscope handling. However, the scans are excellent and reliable for anatomy structures. The technology is constantly evolving and has significant potential for high-throughput studies of biopsies.

2.2. Describe state of the art

The biomechanics of the human body is critical for the performance of physiological functions, as well as for resilience and adaptation in a constantly changing environment. Viscosity and elasticity are indicators of the response of cells and tissues to tension, compression, and regaining shape after applied pressure. The viscoelastic properties of arteries and veins are critical to the functioning of blood vessels, their strength, and the cardiovascular system. Abnormalities associated with a higher water content or thinning of the walls lead to a variety of pathologies, e.g., atherosclerosis, heart disease, and the inability to irrigate the brain. For these reasons, the evaluation of mechanical properties is important. In addition, measurements should be made in a minimally invasive manner. The reason is the structure and sensitivity of biological cells, as well as to avoid causing pain to living individuals.

2.3. Experiments

Hand - held probe. This technique refers to a small and portable device that can measure directly with probes on the patients, which come in various sizes, shapes, and morphologies. Eukaryotic material is highly heterogeneous, and measurements at e.g. a single confocal point might not be representative of properties of a tissue over even several mm. Imaging on the other hand is time consuming, exposing the sample to high amounts of laser energy, which is

undesirable. As such we have designed a hand-held probe that measures the signal from many discrete closely spaced points at the same time and thereby measures an average over a region of a few mm. Applications of such a device can be expected to extend beyond medical diagnostics and span bioengineering and non-biological materials quality control, to determine defects, structural integrity, and hidden anomalies. One of the biggest advantages is its compactness. Probes are easily carried and allow point-of-care diagnostics and onsite inspection, independent of the location. People do not need specific know-how, because of the simplicity of the program, interface, and control. The analysis is cheap, fast, and efficient; it provides real-time data and helps researchers or doctors make their decisions immediately, based on the current assessments. There are some limitations, such as less capability to analyse a large probe; visibility is tricky because of the more complex structure; and the operator should have knowledge to recognise different small parts and make the right interpretation. Calibration and validation procedures should be in place to establish the probe's performance characteristics and maintain consistency across multiple probes or trial sites.

***Brillouin imaging*.** It used an inverted confocal sample-scanning microscope with 40X objective. The laser wavelength was 532 nm. The Brillouin scattered light was collected by the objective and was coupled to a single-mode optical fibre serving as a pinhole. The method includes virtual dispersion and image filters. The final spectral projection is measured on an EM-CCD camera (Hamamatsu ImagEMII) with a spectral finesse of >85. Before each scan, calibration was made with an immersion oil and glue. Scans were controlled by custom software by THATec Innovation (Germany) and analysed with MatLab (MathWorks), based on a phasor analysis (41) or Least squares fitting. For the latter, Stokes and anti-Stokes peaks were fitted with Lorentzian functions. Both results corresponded to each other. Optimal conditions for measurements were 37 °C used.

Tissue preparation. Human tissues were collected from the left upper limb of a male body donor, who had given written consent to donate his dead body. His age at death was 77 years.

The muscles of the proximal forearm and the great subfascial arteries, veins and nerves were exposed using forceps and scalpel. Then 2 tissue samples (~10 × 5 × 5 mm^3) were harvested from muscles with longitudinal fibre arrangement (biceps brachii and pronator quadratus muscle), 2 from veins (brachial and medial cubital vein), 3 from muscular arteries (1 from brachial and 2 from radial artery), and 3 from the median nerve (1 from near its fork, 1 from distal to the pronator teres muscle, and 1 from distal to the carpal tunnel). The tissues were

placed in phosphate buffered saline (PBS) until their further measurement by Brillouin scattering spectroscopy (41).

Sample measurements were conducted using freshly excised tissue samples placed in a heated petri dish containing Phosphate Buffered Saline (PBS) at 37˚C. The measurement process involved positioning the probe directly in contact with the sample. To initiate data acquisition, the camera shutter was opened for the duration of the camera acquisition time, ensuring that the sample was only illuminated for as long as needed. The entire acquisition procedure could be started with a single click of a shutter button, either through the connected computer or manually by the user.

During tissue measurements, the laser power ranged from 10 to 25mW (at the sample), and acquisition times varied from 100 to 750ms. These parameters were adjusted to achieve spectra with satisfactory signal-to-noise ratios (in the shot noise limited regime). Importantly, the range of acquisition times and laser power did not impact the results in terms of inducing any tissue damage or changes. This is consistent with the well-established practice of using comparable laser exposure for significantly longer periods in spontaneous BLS confocal microscopy of live tissue without adverse effects. To ensure the accuracy of measurements, the VIPA spectrometer's dispersion was adjusted so that the BLS peaks covered approximately 10 pixels on the EM-CCD camera. The EM gain was set at a maximum value of 1200. These values can be tailored to optimize the accuracy of BLS peak/linewidth extraction, photon statistics, acquisition times, and other considerations, depending on specific applications or sample characteristics before translation to clinical settings. Each individual measurement was strategically designed to capture the average spectrum from seven points distributed over an approximately 2mm area of the sample, as illustrated in *Figure 5A* inset. This approach effectively minimized the influence of local artifacts that might arise in single-point measurements, providing an averaged spectrum representative of the probed region.

Data was analyzed using a custom Matlab (Mathworks, Germany) code which performed least squares fitting of two Lorentzian curves and spectral registration from reference sample data. Prior to fitting the sample spectra was deconvolved with a measurement of the attenuated elastic scattering peak obtained by holding the probe against a mirror, detuning the gas absorption cell resonance, attenuating the laser with a neutral density filter, and opening the intermediate image plane masks in the spectrometer. These measurements were only performed at the beginning of each measurement session. Owing to the symmetric response

function, deconvolution did not make any noticeable difference to the peak position, and decreased the line width only by a small constant amount. As such, all conclusions from our studies would equally hold for non-deconvolved data. For calibration of the dispersion axis the simultaneously measured spectra of water (7.46 GHZ) and a previously characterized hard plastic (11.30 GHz) were placed in the cuvette on the sample arm in a manner that the detection-excitation area spanned both materials. Calibration spectra were obtained prior to each sample measurement by opening and closing the shutters to the calibration and pointing the probe away from any sample (e.g. to the floor). A single programmed calibration measurement consisted of taking the average of five 500 ms measurements, lasted a couple of seconds, and could be instigated by a single click in the software.

2.4. Explain results

Mechanical characterisation of soft tissue

Figure 5A provides an illustrative depiction of the approximate location of the excised tissue on the arm. The distribution of the measured BLS frequency shift for the various studied tissue types is visually presented in *Figures 5B, 5C,* and *5D.* The complex longitudinal modulus is computed using Equation $M' = \rho(\nu B\ \lambda 0)/2n)^2$, $M'' = M'.\frac{\Gamma_B}{\nu_B}$,utilizing established values from literature for the refractive index and density (1.42 and 1.05 g/cm³ for muscles, and 1.43 and 1.06 g/cm³ for veins and arteries). These results are summarized in *Table 1*.

		ν_B (s.e.) [GHz]	$\sigma_{\nu B}$ (s.e.) [GHz]	M' [GPa]	Γ_B (s.e.) [GHz]	$\sigma_{\Gamma B}$ (s.e.) [GHz]	M'' [GPa]	ν_B [GHz] (probe)	M' [GPa] (probe)
PQM	*Pronator quadratus muscle*	8.190 (0.003)	0.076 (0.003)	2.471	2.480 (0.004)	0.200 (0.004)	0.748	8.213	2.485
BBM	*Biceps Brachii muscle*	8.181 (0.002)	0.063 (0.002)	2.466	2.318 (0.003)	0.152 (0.003)	0.644	8.189	2.471
MCV	*Median Cubital vein*	8.204 (0.001)	0.049 (0.001)	2.469	2.071 (0.001)	0.099 (0.001)	0.623	8.220	2.478
BV	*Brachial vein*	8.260 (0.004)	0.109 (0.004)	2.502	2.617 (0.005)	0.241 (0.005)	0.793	8.264	2.505
RA	*Radial artery*	8.317 (0.001)	0.063 (0.001)	2.537	2.261 (0.005)	0.159 (0.005)	0.796	8.308	2.532
BA	*Brachial artery*	8.363 (0.001)	0.066 (0.001)	2.565	2.262 (0.002)	0.120 (0.002)	0.804	8.371	2.570

Table 1 Mean BLS frequency shift (nB), linewidth (GB) and longitudinal modulus (M', M'') for confocal microscopy scans of different excised human tissue, extracted from Gaussian fits of the distributions. Also listed is the standard deviation of mean (s) for each of these, the standard error (s.e) associated with the fits, and the mean values of nB and M' obtained for measurements using the hand-held probe. (17)

Notably, the analyzed arteries exhibit higher BLS frequency shifts (ν_B) and longitudinal storage moduli (M') compared to the veins, while the veins, in turn, show higher values than the studied skeletal muscles, as indicated in *Figures 5B, 5C,* and *5D*. Distinguishing between specific artery and vein types, both the Brachial artery and Brachial vein stand out with notably higher (ν_B) and M', as depicted in *Figures 5C* and *5D*.

The corresponding linewidth distributions for each excised tissue are also showcased in *Figures 5B, 5C,* and *5D*. These linewidths are connected to the loss modulus (Equation 1) and the longitudinal viscous characteristics, as elucidated below.

To assess the reliability of the handheld probe, we conducted measurements on the same samples using identical conditions. The resulting BLS frequency shift outcomes were then compared to those obtained from the confocal scans (depicted in *Figures 5B-D*), and these comparative results are presented in *Figure 19D*. Remarkably, all measurements obtained with the handheld probe closely align with the mean values derived from the normally distributed values acquired through confocal scans for each sample. Moreover, the standard

deviation across repeated handheld probe measurements (*column 9, Table 1*) is notably smaller than that derived from histograms of confocal scans (*Figures 5*; *column 4, Table 1*). This confirmation underscores the effectiveness of the handheld probe in obtaining spatially averaged values, resilient to potential outliers arising from local spatial variations. The capacity of the handheld probe to yield equivalent average values, compared to a meticulous confocal scan (consisting of numerous pixels), with just a few measurements (five in our case) is evident upon direct comparison of the mean values acquired via the two detection methodologies, showcased in the inset of *Figure 19D*. Rigorous statistical analysis of the handheld probe measurements (*Figure 19D*) corroborates its capability to reliably distinguish between different tissue types.

The handheld probe further proves valuable in detecting variations in properties of the same tissue type across distinct locations. This is exemplified in *Figures 6A-E*, where the BLS frequency shift and linewidth of the Brachial/Radial artery (BA/RA) and Median nerve (MN) are measured at different arm positions (indicated on the diagram in *Figure 6A*). Observations in *Figures 6B* and *6D* indicate a slight increase in BLS frequency shift (ν_B) for the artery as it progresses up the arm (towards the torso), while no significant alteration is discerned for the nerve. Alterations in linewidths (Γ_B) relative to frequency shifts (ν_B) are visualized in *Figures 6C* and *6E*. These plots, unveiling the scaling of viscous longitudinal properties against elastic longitudinal properties, display distinct trends in the two tissues (Pearson correlation coefficient of 0.46 versus -0.53), potentially suggestive of differing underlying mechanical relaxation time spectra, as discussed subsequently.

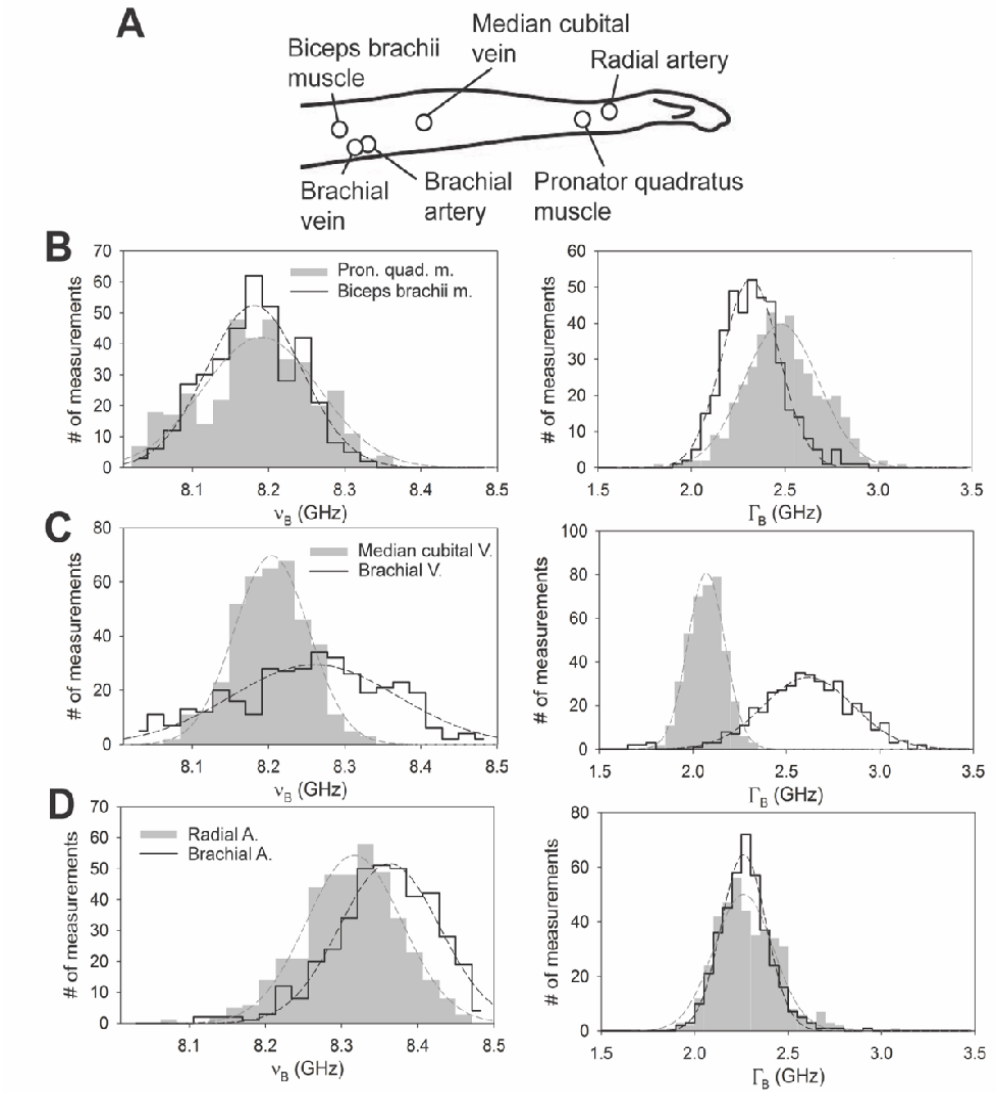

Figure 5(A) Sketch showing approximate location on arm of the excised tissues studied. (B-D) Distribution of BLS frequency shift (ν_B) and linewidth (Γ_B) for the different tissue samples obtained from large-area confocal grid scans. Taken from Ref (17)

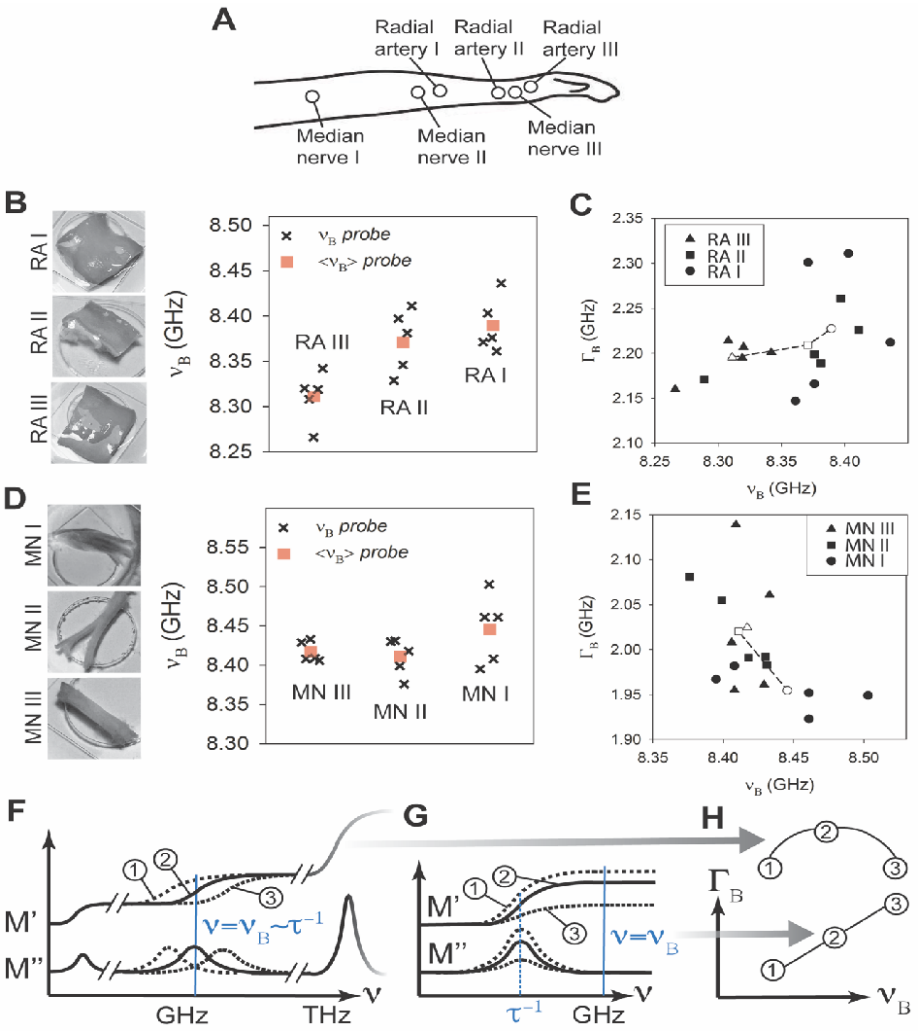

Figure 6(A) Sketch showing approximate locations along the arm of the excised tissues studied. (B & D) Collated results of independent measurements of νB (x) using the hand-held probe at different positions of the Aorta Radialis (AR) and Nervus Medianus (NM) as indicated in "A" (n = mean of 5 measurements). (C & E) Corresponding plots of ΓB vs νB. (Solid symbols = individual measurements; open symbols = mean; dashed line = trend line of mean). (F) & (G) Expected frequency dispersion of the complex modulus $M = M' + iM''$ when probing (F) a heterogeneous sample with different relaxation times (t) in the vicinity of $\tau \sim \nu_B^{-1}$, and (G) the effect of different strengths of a relaxation process with $\tau > \nu_B^{-1}$ as may occur for different solid fractions. (H) Sketch of the expected scaling of Γ_B with respect to ν_B for the two scenarios. Taken from Ref (17)

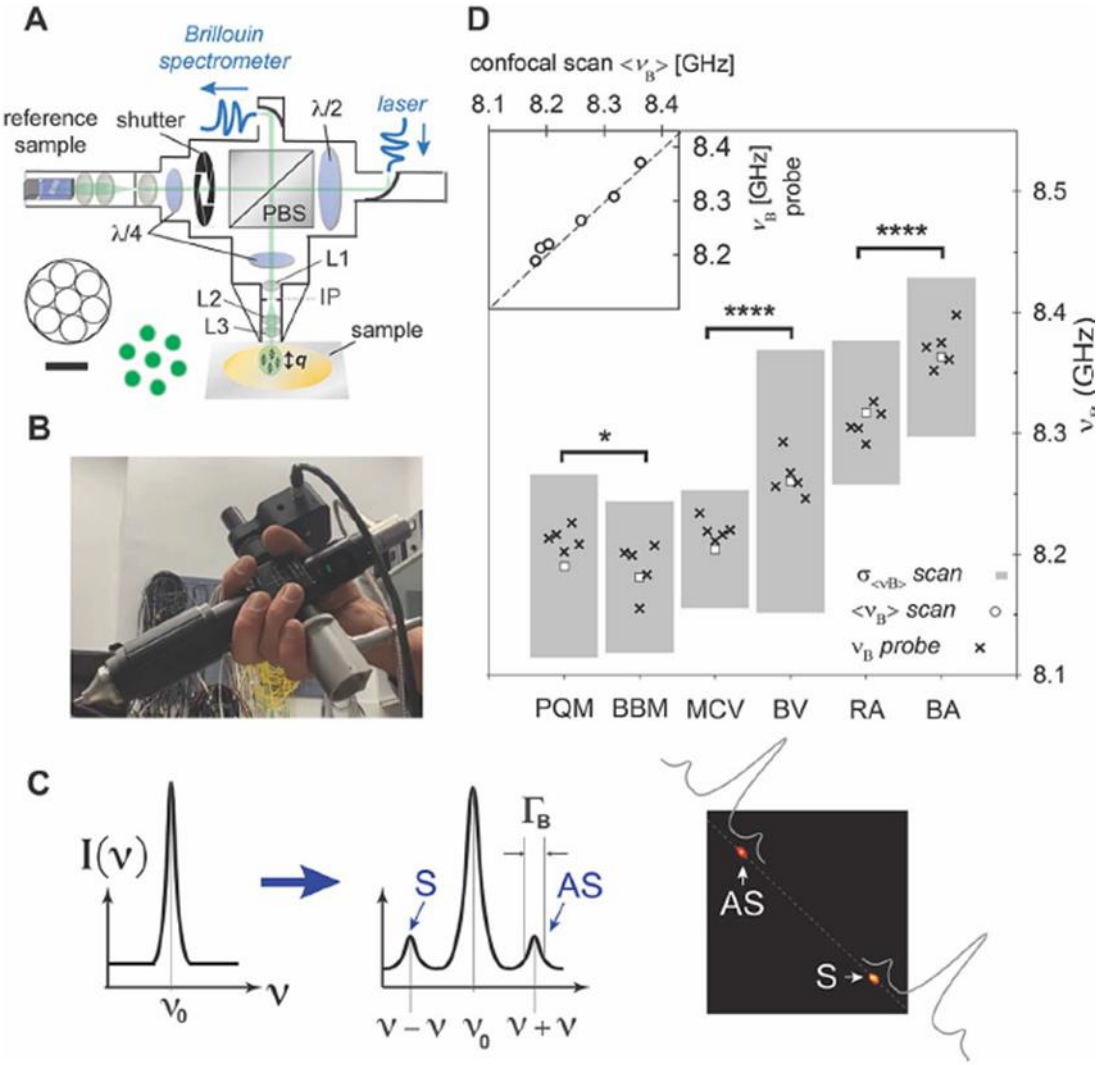

*Figure 19 (A) Schematic of the hand-held BLS probe (PBS = Polarizing Beam Splitter; k/4 = quarter waveplate; k/2 = half waveplate; IP = intermediate image plane; L1 & L2 relay lenses; L3 focusing lens; q = predominant phonon-scattering wavevector probed in the sample). Inset shows a sketch of the multimode fiber bundle cross section used for coupling light into and out of the probe, and the excitation pattern projected onto sample (green dots). Scale bar = 1 mm. (B) Photograph of hand-held probe. (C) Example of BLSspectra showing Stokes (S) and Anti-Stokes (AS) BLS scattering peaks shifted by frequencies ±mB relative to the probing laser frequency m0. Also shown is an example of a raw spectral projection measured with the BLS imaging spectrometer using the hand-held probe (dashed line = dispersion axis). (D) BLS measurements on the same samples as in Figure 5 using the hand-held probe (x). Also shown are mean values (h) and the standard deviation of the mean (grey bars) of the confocal scan measurements (viz. Fig. 5 and Table 1). Inset: Mean mB obtained from confocal scan measurements versus that obtained using the hand-held probe (later is average of 5 measurements). Statistical differences are for mB of the different tissues measured using the hand-held probe, and were performed using unpaired t-test's with Welch's correction (*p < 0.05, ****p < 0.0001). Sample acronyms are as defined in Table 1.* Taken from Ref (17)

2.5. Discussion

Among the measured samples, it becomes evident that arterial walls exhibit a higher storage modulus (M′) compared to veins, which, conversely, display a higher modulus than skeletal muscle tissue. With the exception of the Median cubital vein (MCV), the loss modulus (M″)

showcases a contrary trend. It is a recognized fact that veins possess greater compliance than arteries, signifying a higher capacity for deformation under a given pressure (33,48). This observed reduction in M′ may potentially reflect this inherent disparity in compliance. Additionally, it is noteworthy that prior quasi-static tensile and shear assessments have also indicated augmented arterial modulus in contrast to veins, further surpassing that of skeletal muscles (49). Our findings underscore that the BLS frequency shift (νB) for nerves (as depicted in Figs. 6D and 6E) is significantly larger than that of skeletal muscles, veins, and arteries. This tendency extends to the lower frequency shear and tensile moduli (46). In this regard, for all probed tissue types, M′ follows a similar pattern to the quasi-static tensile storage modulus. However, this parallel behaviour between the low and high frequency properties requires careful interpretation due to differences in factors such as boundary conditions and frequency regimes associated with BLS measurements. Nonetheless, it could be argued that load-bearing components in solid-like tissue possess characteristic mechanical relaxation times significantly slower than the probed gigahertz frequencies. Thus, alterations in solid structure or constituent abundance might manifest themselves in both BLS-measured and quasi-static tensile moduli, albeit with the latter being influenced also by the substantial liquid bulk contributions.

The efficacy of the hand-held probe to provide averaged spectra across an extended area is convincingly demonstrated in *Figure 5 B-D*, where all measurements closely align with the mean obtained from conventional confocal scans (inset of *Fig. 19A)*. These measurements also successfully differentiate between distinct tissues (*Fig. 19A*), a task unattainable through single-point measurements. This capability proves particularly vital when dealing with heterogeneous soft tissue, where BLS spectra could exhibit spatial variation yet maintain only minor differences in average values between samples. Notably, the presence of mechanical property heterogeneities is not confined to BLS and is also evident in other techniques such as Atomic Force Microscopy (AFM). Although distributions in *Figure 5* are well-described by normal distributions, suggesting a sufficient number of data points to account for tissue heterogeneity, the Pronator quadratus muscle and possibly the Brachial artery hint at potential bimodal distributions. These features are not evident in handheld probe measurements, which consistently yield values close to the single-distribution mean (*Fig. 19D*). This indicates the handheld probe's efficiency in averaging out spatial heterogeneities.

Our handheld probe's results further demonstrate its capability to detect variations in the BLS modulus within the same tissue at different locations. For instance, the Brachial/Radial artery

displays an increased BLS frequency shift (ν_B) as one moves up the arm (*Fig. 6B*), conceivably related to higher pressures experienced by larger arteries. Conversely, the Median nerve displays no such discernible trend (*Fig. 6D*). Analyzing the scaling of longitudinal elastic to viscous properties (evidenced by plotting νB against ΓB) highlights a notable distinction between the Brachial/Radial artery and the Median nerve (*Figs. 6C* and *6E*). To deduce the origin of this distinction concerning the mechanical relaxation spectrum necessitates systematic sample perturbation (e.g., temperature, hydration changes) or correlative measurements at various frequencies, endeavours beyond the scope of this proof-of-principle study. It's important to acknowledge that a decrease in the BLS linewidth relative to the frequency shift (as seen for the Median nerve, *Fig. 6E*) may stem from the BLS-probed frequency being slightly above a prominent relaxation process ($\nu B > \tau^{-1}$, where τ represents the characteristic relaxation time). Conversely, an increase in the BLS linewidth concerning the frequency shift (as observed for the Brachial/Radial artery, Fig. 6C) could stem from being just below such a relaxation process ($\nu B < \tau^{-1}$) or a relative enhancement in a solid component with a slower characteristic relaxation time, applicable to different hydration levels. The effects of the latter scenario on the frequency dispersion of the complex modulus M and the ensuing M″/M′ scaling are depicted in *Figs. 6G* and *6H*.

Numerous studies have suggested the potential medical diagnostic value of the BLS modulus. For instance, BLS confocal microscopy studies on carotid arterial histological sections have unveiled sensitivity to plaque stiffness in mouse models (3). Likewise, investigations on muscle fibrils have revealed correlations with functional loss attributed to specific mutations (42). A comprehensive study encompassing diverse tissues has also distinctly differentiated between tissue types, implying applicability in diagnosing pathological anomalies on a broader scale (40,43). Speculatively, given the distinct BLS moduli of collagen and elastin (47), BLS could offer a measure of age-related arterial "stiffening," related to increased collagen-to-elastin ratios. The similarity between BLS-measured M′ and quasi-static tensile modulus trends encourages exploration into BLS sensitivity to disease progression, such as atherosclerosis, which is linked to alterations in collagen network morphology, detectable via AFM (15). For such applications, the presented probe could provide a practical advantage, potentially enabling direct clinical application without the need for excision. Notably, our study's tissue samples were freshly excised, placed in isotonic media at 37 °C, closely resembling their natural state. Consequently, variations due to hydration, critically sensitive to BLS, would mirror those seen in native living tissue. Our outcomes emphasize what could reasonably be anticipated in situ studies.

While we have predominantly focused on the BLS frequency shift (νB) and M′, as opposed to the linewidth (ΓB) and M″, comprehensive examination of the latter could provide a promising future research avenue. The increasing recognition of M″, despite its complexities in extraction using imaging spectrometers, is underscored by its pronounced relative changes, often surpassing those of M′ in soft matter (19). This is evident in *Figures 5B-D* and *Figures 6C* and *E*, as well as from theoretical considerations of the M″ dispersion (*Figures 6F-H*). Notably, M″ is tied to the longitudinal viscosity ηL through $M'' \approx 2\pi\nu B\, \eta L$, where $\eta L = \eta B + (4/3)\eta S$, and ηB represents the bulk viscosity. This distinguishes ηL from shear viscosity ηS, with ηB's significance being for high-pressure/impulse deformations or longitudinal wave propagation. While ηB would predominantly impact deformations under high pressures, it likely holds minor significance for physiological deformations in soft matter. Given that ηB is of a similar magnitude as shear viscosity, relative variations in ηL largely mirror changes in ηS. As such, despite gigahertz frequencies for quasi-static elastic properties, ηL might serve as a proxy for changes in viscous properties under physiological conditions.

The probe's sensitivity ultimately hinges on fibre coupling efficiency. Our routine success rate exceeds 50%, though this is subject to wavefront deformations induced by the sample and hence tissue-specific. It is important to underscore that our findings stem from multiple measurements across diverse tissue regions within a single individual. While this initial phase is critical for the development and refinement of appropriate probes, the attainment of comprehensive conclusions necessitates data collection from a broader sample of individuals.

2.6. Conclusion and importance of results

In conclusion, we have introduced and successfully demonstrated the viability of a robust handheld Brillouin Light Scattering (BLS) probe for the examination of various freshly excised human tissues. This versatile tool holds potential not only for anatomical studies but also for potential clinical applications. A standout feature of the probe is its ability to capture average spectra across a wide spatial area in a single rapid measurement lasting less than a second. This is achieved by illuminating a pattern of spots on the sample, yielding a νB value that closely aligns with the mean obtained from more time-consuming confocal microscopy scans of the same samples. This single-shot measurement capability, coupled with minimal laser exposure, enables the discrimination of distinct tissue types—a feat challenging to accomplish through point measurements due to the heterogeneous nature of many tissues.

While our current implementation covers an approximate 2 mm diameter probing area, adjustments in the relay lens focal length can readily modify this area, catering to specific applications. It's worth noting that for some applications, the instant averaging property of our probe might not be ideal, necessitating more intricate scanning probes. Although our study primarily aimed at a proof-of-concept demonstration of the handheld probe, we have gleaned insights into tissue properties that could lay the foundation for future investigations. Notably, our findings regarding vasculature suggest an increasing storage modulus (M′) as one moves towards the upper arm (closer to the torso). Furthermore, the observed BLS moduli for skeletal muscles, veins, arteries, and nerves appear to mirror trends observed in quasi-static tensile measurements—largest for nerves and smallest for skeletal muscles. Despite the discernible differences in the probed moduli, this convergence is promising as it suggests that BLS-measured modulus variations could potentially serve as indicators of pathological anomalies associated with alterations in quasi-static tensile mechanical properties. Nonetheless, the extent to which BLS can effectively contribute to tissue health classification and pathology assessment in clinical settings remains to be thoroughly explored. The handheld probe we introduced provides a valuable tool for further in situ investigation of these possibilities.

Broader importance of studying nuclear mechanics: In medicine, nuclear mechanics influence tissue regeneration and disease treatment. Changes in shape, stiffness, and function are linked to cancer development—the leading cause of 21st-century mortality according to the World Health Organization (21). A deeper comprehension of mechanical properties and nuclear dynamics aids in early diagnosis, prevention, and the identification of harmful factors. Additionally, it can potentially lead to new therapies and medications that address the mechanics (rather than purely the chemistry) which extend patients' lives.

The study of nuclear mechanical properties poses challenges. Not only is the nucleus very small, but most techniques involve physically impacting and altering shape to observe recovery (18) . This may affect the mechanics in itself Jitao Zhang's recent study (62) confirmed changes in the longitudinal modulus can be observed in the cell nucleus for different chromatin states, which are related to transcriptional activity.

The nucleus is however a highly dynamic structure. Its dynamic properties are key to its functions and worthy of study if one wishes to mechanistically understand what goes wrong in diseases. Here we explore whether Brillouin microscopy can potentially provide a useful

tool for studying dynamic changes in the nuclear mechanics, and what these can tell us about how it works.

Chapter 3: 3.1. Nucleus

The cell nucleus locates in the centre of the cell. Its size varieties 5 to 20 µm. It plays a key role in vital cellular functions for genetic transcription and reproduction (24,38). In eukaryotic organisms, compartmentalization is evident, segregating distinct functions into various spatial domains. Chromosomes, composed of chromatin, interact with genes located in the nuclear interior, while inactive ones often localize to the periphery (24). This positioning is contingent upon size and gene density (19). Physical alterations and replacements can trigger DNA damage within nuclei, resulting in a loss of coherence of chromatin compaction (22). This phenomenon significantly influences hybridizations, crossing-overs of chromosomes, and a reduction in their condensation (20). Given the size of mammalian nuclei, the spatial resolution of Brillouin microscopy is adequate for studying the internal mechanics of the nucleus. Indeed, Brillouin microscopy has recently been used to show that condensed and decondensed chromatin have distinct elastic moduli (62). While this study has convincingly shown the sensitivity to chromatin state it has not explored the dynamic behaviour (namely how the chromatin mechanics changes over time). Nowadays, there has been much interest on the dynamic properties of chromatin, with evidence that it undergoes state oscillations on the scale of several seconds (32), and exhibits spatially coherent dynamics on the micron scale (25). Studies of the sub-second dynamic changes are possible using our Brillouin microscope.

Recently it was shown that these oscillations are also reflected in the anisotropy of the mechanical properties in the nucleus (17). In this study a reaction-diffusion type model was proposed to describe chromatin state oscillations, which predicts that these should be accompanied by fluctuation in the ionic concentration/pH (*Fig.7*).

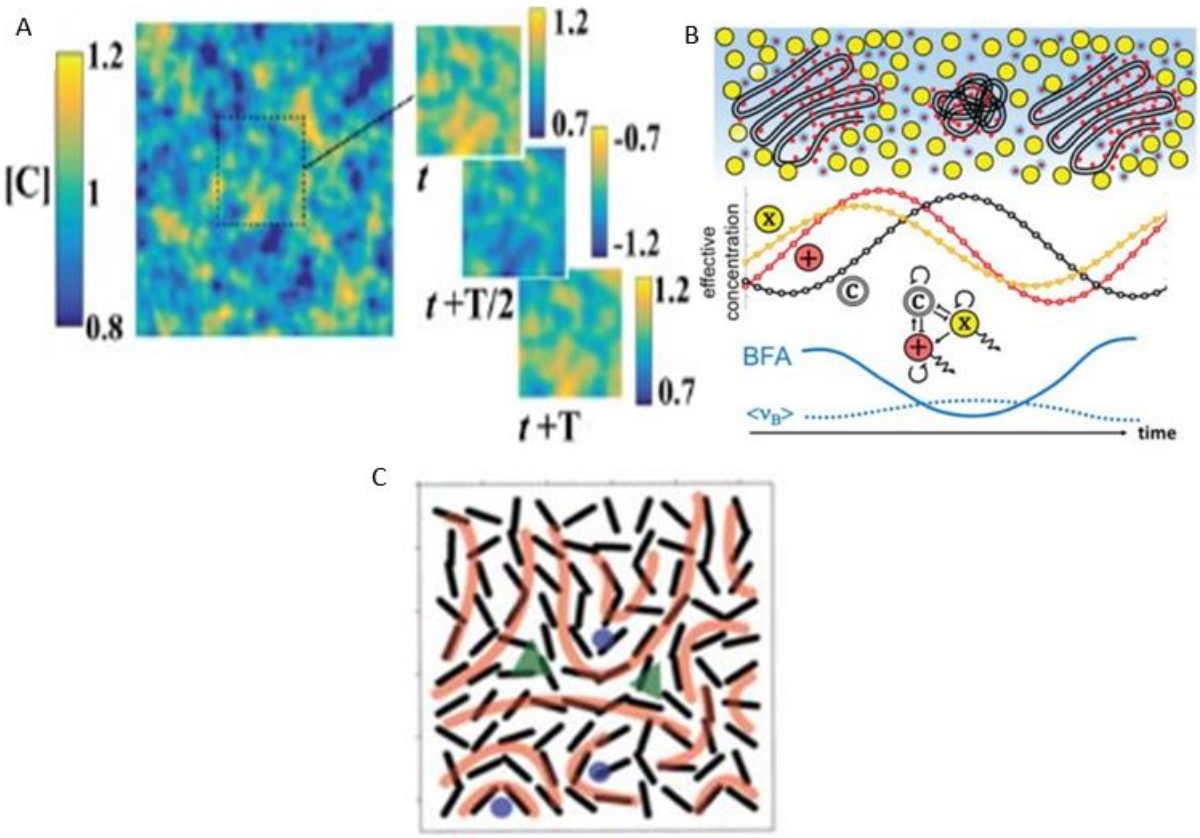

Figure 7 (A) shows a model for oscillations (B) Chromatin fluctuation, 2 diffusing species, with a larger/smaller diffusion coefficients that promote/inhibit condensation with stable spatio-temporally oscillating solutions SSOS (C) Orientational BLS mechanical order like quasi-nematic liquid crystal near a critical order-disorder transition. Taken from Ref (17)

Here in this section we explore whether such oscillations are also observable in the Brillouin frequency shift (which according to the model should also exhibit subtle oscillations in living cells). A secondary goal is to see if these are also correlated to ionic concentration oscillations predicted. In principle the phase difference between the ionic concentration and Brillouin frequency shift should allow us to calculate important parameters of the model such as the diffusion (and hence size) of molecules that promote/inhibit chromatin condensation/decondensation (25) (*Fig.8*).

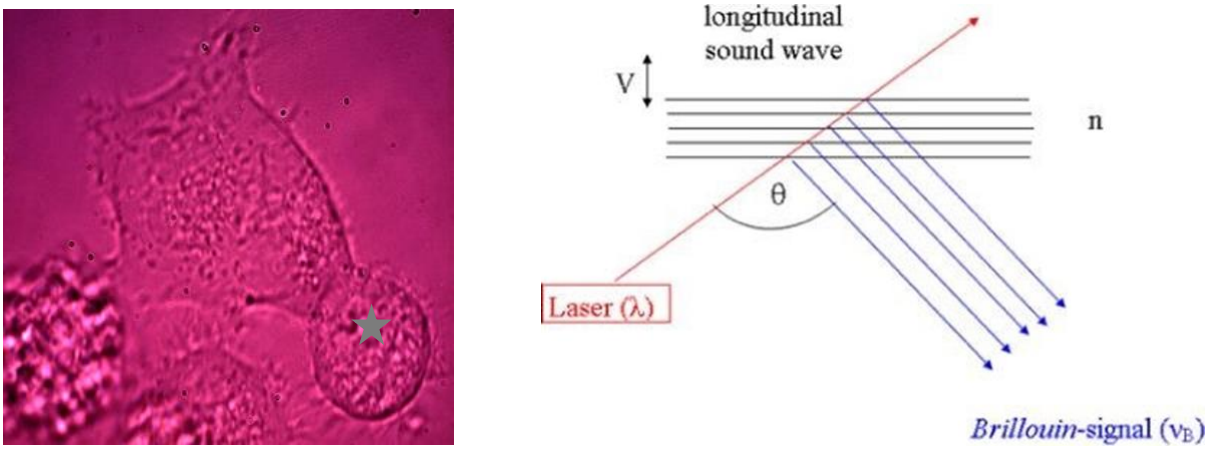

Figure 8 (A) Point of measurement on widefield image. (B) Schematic representation of Brillouin scattering. Taken from Ref (23)

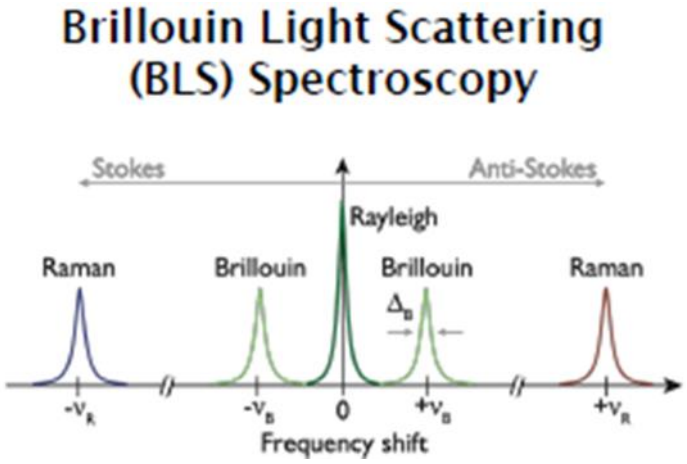

Figure 9 BLS works by focusing a single frequency laser at sample and measuring wavelength-change of scattered light. This is tiny: Dl<0.1nm Dk<0.1 cm-1 and requires special spectrometers. Taken from Ref (24)

In its wavelength-resolved form, it involves focusing a single-frequency laser onto a sample point and measuring changes in scattered light wavelength (*Fig.8*). Brillouin scattering refers to the interaction of light with the waves in a medium stuff. *Fig. 9* represents how the spectrum looks like. This method is advantageous as an all-optical and label-free technique and can spatially map a sample with high resolution (<200nm).

Figure 10 illustrates the operational principle of Brillouin microscopy as applied for measuring mechanical properties within the nucleus. It can be utilized to discern subcellular structures based on mechanical properties and interactions between the nucleus and cytoskeleton (18). M' decreases by 1.81% under the influence of TSA, which can be attributed to chromatin decondensation.

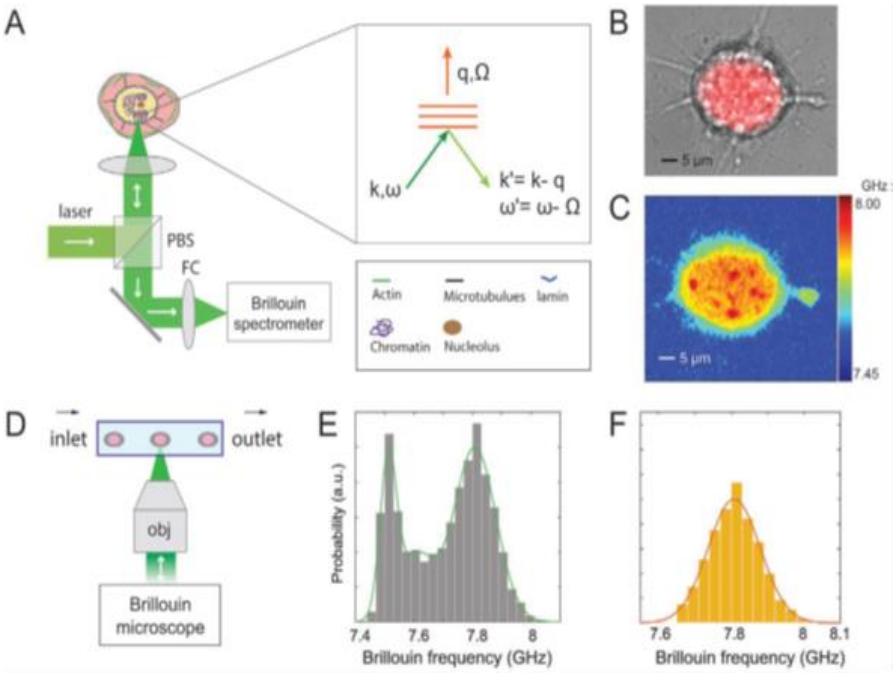

Figure 10 Characterization of nuclear mechanics with Brillouin technique. A) Principle of using a confocal Brillouin microscope to measure nuclear mechanics of a cell. The light red and yellow regions indicate cytoplasm and nucleus, respectively. (inset) the phase-matching condition indicates that the induced Brillouin frequency shift is equal to the frequency (a few GHz) of hypersonic acoustic waves Ω. ω and k represent the frequency and wave vector of incident light, and ω' and k' are the frequency and wave vector of scattered light, respectively. B) co-registered bright-field and fluorescent image of a cell with its stained nucleus. C) corresponding Brillouin image of the same cell. The colour bar has a unit of GHz. D) schematic of Brillouin flow cytometry. E) original flow data of cell population with the fitting of the histogram's profile. F) extracted signature of the nucleus. The details of the data extraction procedure are provided in the Experimental Section.
Taken from Ref (62)

3.2. Describe state of the art

The nucleus plays a vital role as the cell's command centre, orchestrating genetic transcription and ensuring proper cellular development, proliferation, and overall organismal function. Understanding the nucleus's physical mechanisms is crucial for comprehending diseases linked to its dysfunctions (e.g., cancers, neurodegenerative disorders, genetic anomalies) and differentiating between living and non-living systems. In eukaryotic cells, the nucleus is a dynamic organelle characterized by various levels of order. It can exhibit both liquid-like and solid-like attributes and can be likened to a dense polymer solution or "soup," with chromosomes as the polymers (*Figure 11*).

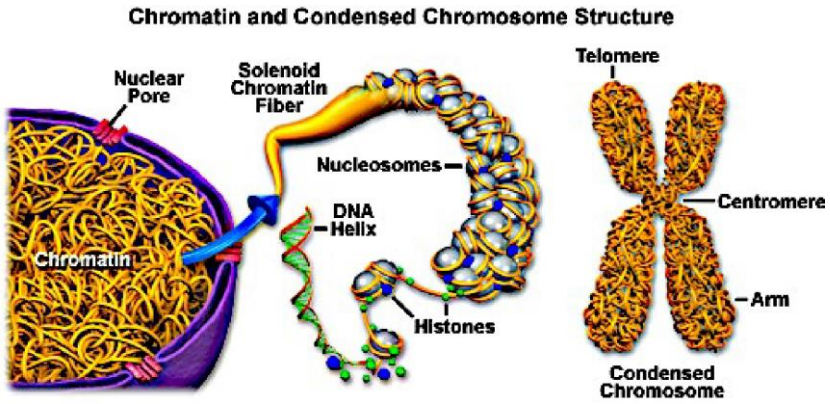

Figure 11 The nucleus in eukaryotic cells, is a heirarchical structure often described as a dense polymer soup (the polymers being chromatin) Taken from Ref (22)

While these polymers are organized into territories with dynamic boundaries, our comprehension of how the nucleus sustains and adjusts its internal structure in relation to function remains limited (26,32). The nucleus's chemistry involves DNA organized into chromatin strands that transition between compaction states linked to transcriptional activity. Numerous active chemicals, some not fully understood, control chromatin state and function, along with passive processes influenced by ions and molecular crowding. These factors are complex to disentangle, leading to a superficial grasp of their roles in nuclear processes. Non-perturbative measurements of these dynamics are challenging, and we lack dynamic maps of factors like cation concentrations that impact chromatin state.

Mechanical properties, alongside chemistry, underlie any physical change (e.g., chromatin polymer state and configuration). These properties, involving both structures and their interactions with surroundings, are vital. The mechanical characteristics of chromatin, which can change heterogeneously during cell cycles, are expected to be highly dynamic, given coordinated intra-nuclear translational and state dynamics (56).

The nucleus behaves as a liquid on readily observable timescales (>ms) due to its high water content (>70%). However, studying its structural formation necessitates examining ultra-short timescales, where viscoelastic materials, including biological matter, exhibit solid-like behaviour. We aim to measure this solid-like behaviour to unravel how it leads to the complex, dynamic, and coordinated structure seen on longer timescales. Furthermore, understanding of the role of different molecular species', their interactions and interdepence holds potential for personalized disease treatments (as mentioned above).

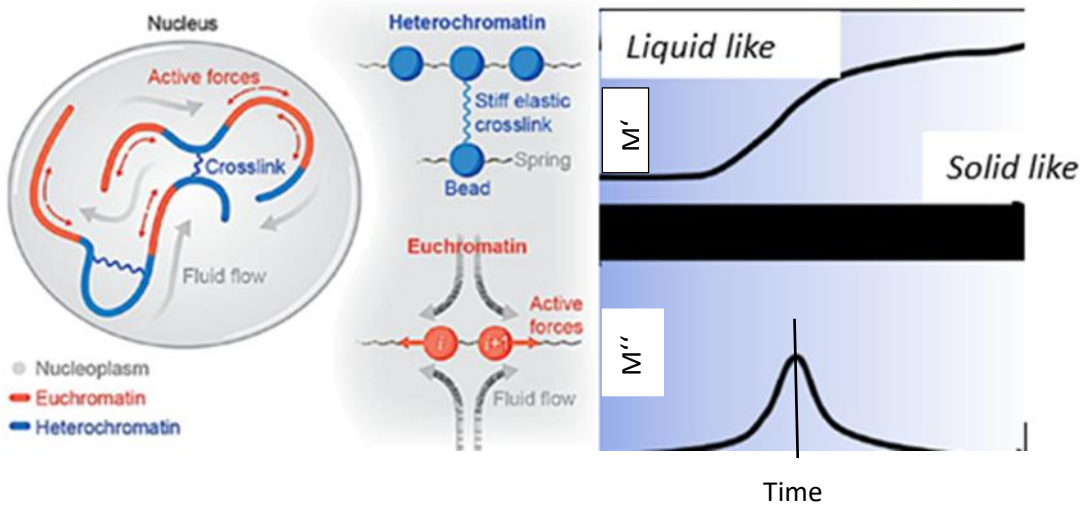

Figure 11.2 Since the nucleus is effectively a liquid Taken from Ref (24)*(>70% water) at time-scales of functional changes (>ms), coherent properties are odd. Structure can however form at short time scales (ps-ns) , where it is more solid-like.*

The left side of the *Fig. 11.2* is an illustration that cross-linking between chromatin may occur. This can be argued to affect the mechanics (especially at higher frequencies) since it is a transient process in the nucleus. The right side on the other hand shows how the storage and loss modulus scale with frequency. The vertical line, goes to the peak in the loss modulus, indicate where we are measuring with Brillouin microscopy. It can presumably be sensitive also to the degree of cross-linking. Spontaneous light scattering spectroscopy directly measures elastic and viscous properties on picosecond-nanosecond timescales.

The reaction-diffusion model suggests an oscillating chromatin state around ~0.1Hz, out of phase with the cation concentration oscillation but de-phased temporally. A decrease in available cation concentration may disrupt the stable oscillatory state, with an active restoring mechanism initially dampening oscillation magnitude and establishing a new equilibrium. Increasing diffusion coefficients could similarly perturb equilibrium, leading to increased spectral noise.

3.3. Experiments

Brillouin imaging. An inverted confocal sample-scanning microscope with a 40X objective was utilized for the experiment. The laser employed was a 532 nm wavelength laser. The Brillouin scattered light collected by the objective was directed into a single-mode optical fiber, which functioned as a pinhole. The approach involved virtual dispersion and image

filters. The resulting signal was then channeled to a multiplied camera, specifically an EM-CCD camera (Hamamatsu ImagEMII), boasting a spectral finesse exceeding 85. Calibration was performed prior to each scan using immersion oil and glue. Cell scans were facilitated by THATec Innovation, and the images provided determinations for specific areas. Data analysis was conducted using MatLab (MathWorks), employing a phasor analysis. The Stokes and anti-Stokes peaks were fitted using Lorentzian curves, yielding consistent results. The peak frequency identified through Brillouin microscopy indicated local stiffness. Optimal measurement conditions were achieved at 37°C and 5% CO2.

Cell preparation. For the experiments, rat fibroblasts and HeLa cells were employed. To create a suspension, cells were detached using 0.25% Trypsin-EDTA (Thermo Fisher Scientific), centrifuged, and then re-suspended in a phosphate-buffered saline (PBS) solution without Mg2+ and Ca2+. The final cell concentration ranged from 105 to 106 cells per ml.

HeLa cells were selected due to their easy and rapid cultivation, as well as their availability. They mimic live cancer cells found in the cervix and have been extensively studied (3).

These cells were plated on high-precision glass-bottom dishes and observed using an inverted microscope configuration. Widefield transmitted light images were utilized to identify viable isolated cells based on their morphology.

To study temporal oscillations in the picosecond-scale elastic properties, a single-frequency (532nm) laser was focused at the cell nucleus's central position (NA=1.3). The Brillouin scattering signal was detected using a custom-built confocal VIPA-based Brillouin Light Scattering spectrometer. The effective detection pinhole corresponded to approximately 1 Airy Unit, ensuring a measurement volume of 200-300nm (laterally) and 600nm (axially).

Continuous time-traces of spectra were captured at 300ms intervals for about 5000 time points. Laser intensity remained at levels (<10mW) previously demonstrated not to impact cellular processes in this cell type during these acquisition times. After spectral registration with control samples, each spectrum was fitted using custom Matlab software to reveal the temporal evolution of the Brillouin frequency shift, directly related to the square root of the picosecond longitudinal elastic modulus.

Outliers resulting from poor spectral fits were removed from the time traces, and spectral decomposition was calculated using a fast Fourier transform. The data were subsequently analyzed for characteristic spectral components in the range of approximately 0.1-1 Hz above the noise background.

These experiments were conducted at various temperatures (30°C, 33°C, 35°C, 37°C, 39°C, and 41°C) and with different dilutions of the PBS buffer (100%, 75%, 50%, and 25%). For the latter, the buffer was replaced with the respective dilution while the cells were on the microscope stage. The point of analyzing different temperatures is to influence the thermodynamic conditions and diffusion coefficients of molecules. Due to the nuclear membrane's ionic permeability, this perturbation effectively reduced the concentrations of K+ and Na+ ions by percentages corresponding to the dilution. For each perturbation, the cells were allowed to stabilize for 5 minutes, ensuring they reached thermodynamic equilibrium and the nuclear cation concentration equilibrated (or reached a quasi-stable state).

3.4. Explain results

Figure 12.1 demonstrates the steps of measurement and analysis. *Figure 12.1A* shows the raw data spectra of the oil and glue controls, along with their fits on the left. A plot of the fitted signals is displayed on the right for both Stock and anti-Stock. It is crucial that the signals fit together in both positions to ensure correct measurement. In *Figure 12.1B*, we observe the raw BLS spectrum data over a period of time. Each point represents a measurement corresponding to a specific BBS concentration or temperature, and white noise caused by external factors is also present. *Figure 12.1 C* reveals the transformed signal, which allows us to interpret the results and draw corresponding conclusions.

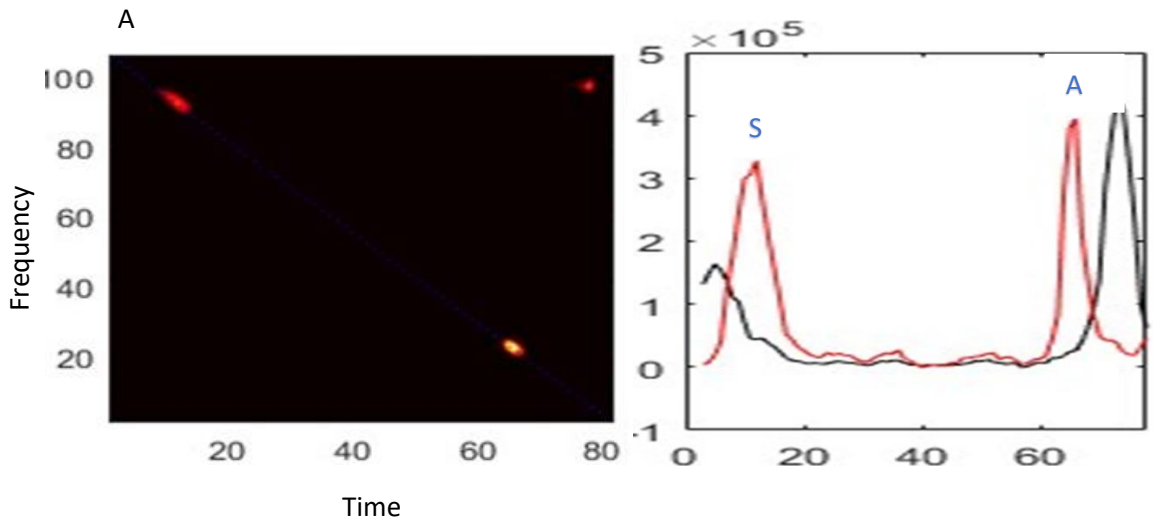

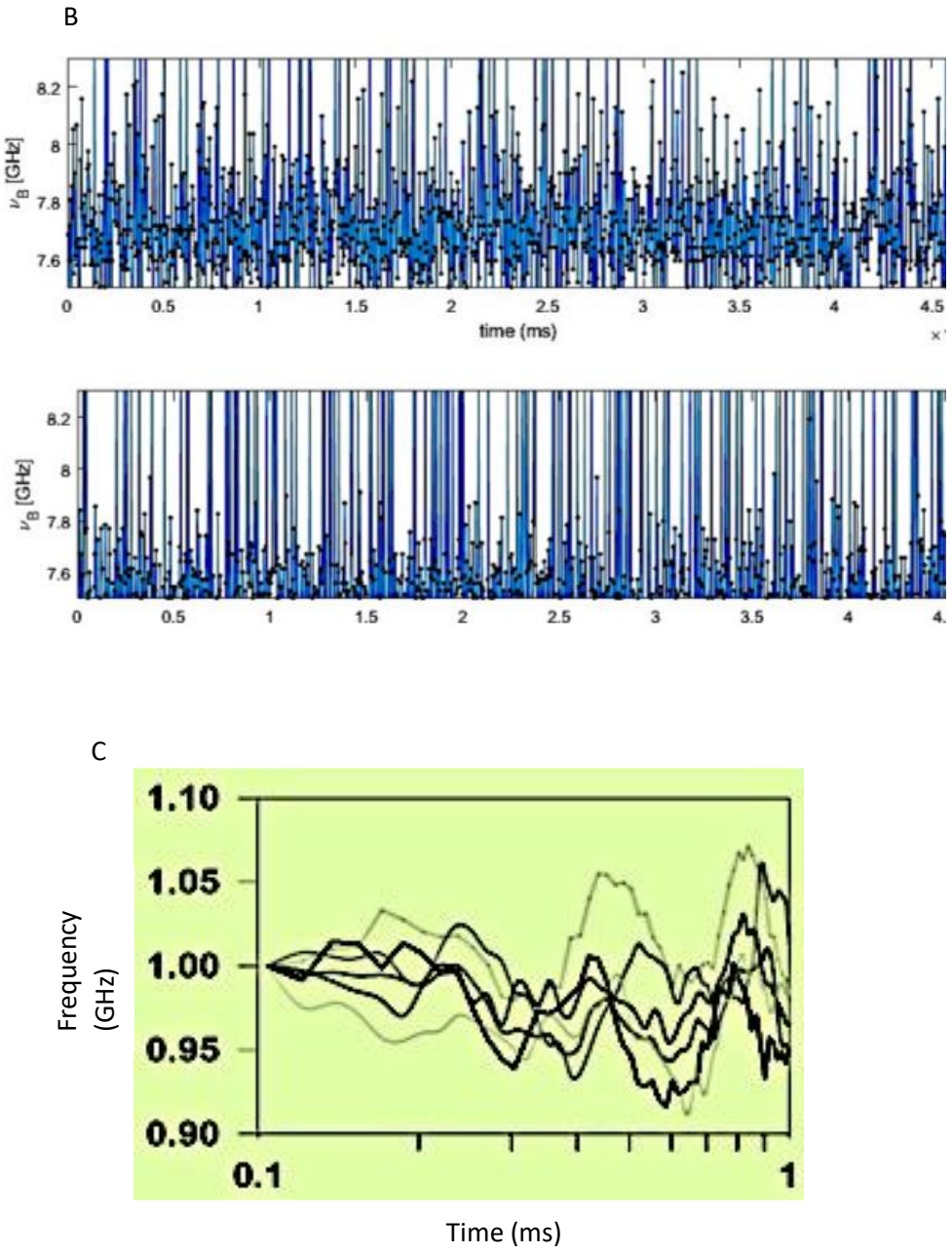

Figure 12.1 BLS frequency shift over time. (A) demonstrates the row BLS control spectrum. 532nm laser focused at a central position in cell nucleus (NA=1.3) and BLS signal measured with confocal 2- VIPA BLS spectrometer. Pinhole ~1 AU (effective PSFxy=200-300nm/PSFz=600nm. Laser intensity <10mW) (B) shows plot of BLS over time. Time-traces for ~5000 time points with 300ms exposure/spectra. (C) After spectral registration, spectra were fitted to give nB-time traces and FFTs calculated.

PBS concentration

Figure 12.2 shows the power spectrum of fluctuations in the Brillouin frequency shift in a HeLa cell nuclei and cytoplam at 37°C with 100% PBS concentration. As can be seen the former shows a distinct power spectrum with an enhanced contribution at ~0.2Hz. (*Fig. 12.2* shows spectral decomposition in the nuclei).

Fig. 13 exhibits representative power spectral decompositions in 3 different nuclei at 37°C, 100% (first column), following a perturbation in the form of a 50% decrease in PBS concentration (second column), compared to that in the cytoplasm (third column). As can be seen the PBS concentration perturbation appears to decrease the defined spectral feature at ~0.2 Hz which are also not present in the cytoplasm. *Fig. 14* show the spectral decomposition for different PBS concentrations at 37°C (average of measurements on 5-18 cells in each case). Here it can be seen firstly that fluctuations of a characteristic frequency are attenuated as the PBS concentration is initially decreased. There is also a clear increase in the spectral white noise as can be seen by the higher plateau seen in the frequency range above ~0.1 Hz. This suggests that at non-homeostatic conditions the cells lose their ability to suppress the "random" noise, which can bury characteristic frequency oscillations. This loss of temporal coherence is what one would expect when a stable oscillatory state is driven out of its quasi-static equilibrium. *Fig. 8* and *Fig. 9* represent the model, taken from (17). We may quantify this effective enhancement of white noise away from homeostatic conditions by fitting the spectra with a simple exponential function and looking at the characteristic coherence time (tc), which is seen to drop approximately exponentially with decreasing PBS concentration (*Fig. 15*). It would be interesting to see how this would scale for K+ and Na+ concentrations above the homeostatic values (i.e. concentrated PBS) and whether this similarly results in an increased noise spectrum. It would also be interesting to see the temporal evolution of this increasing noise spectrum following a change from homeostatic conditions (not investigated here), which can give further insight into the nature of the stable oscillatory state and potentially predict critical exponents (17).

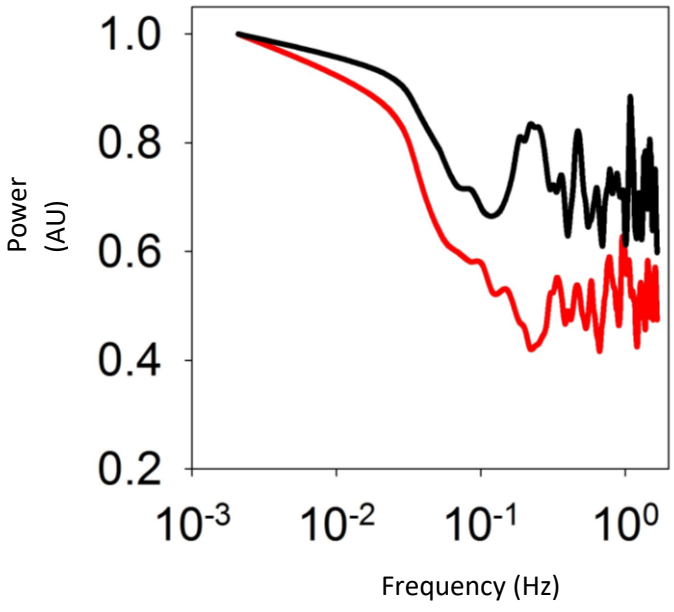

Figure 12.2 Spectral decomposition of BLS fluctuations in nuclei (black), cytoplasm (red) 532nm laser focused at a central position in cell nucleus (NA=1.3) and BLS signal measured with confocal 2-VIPA BLS spectrometer. Pinhole ~1 AU (effective PSF xy=200-300nm/PSF z=600nm. Laser intensity <10mW). Time-traces for ~5000 time points with 300ms exposure/spectra. After spectral registration, spectra were fitted to give vB-time traces and FFTs calculated.

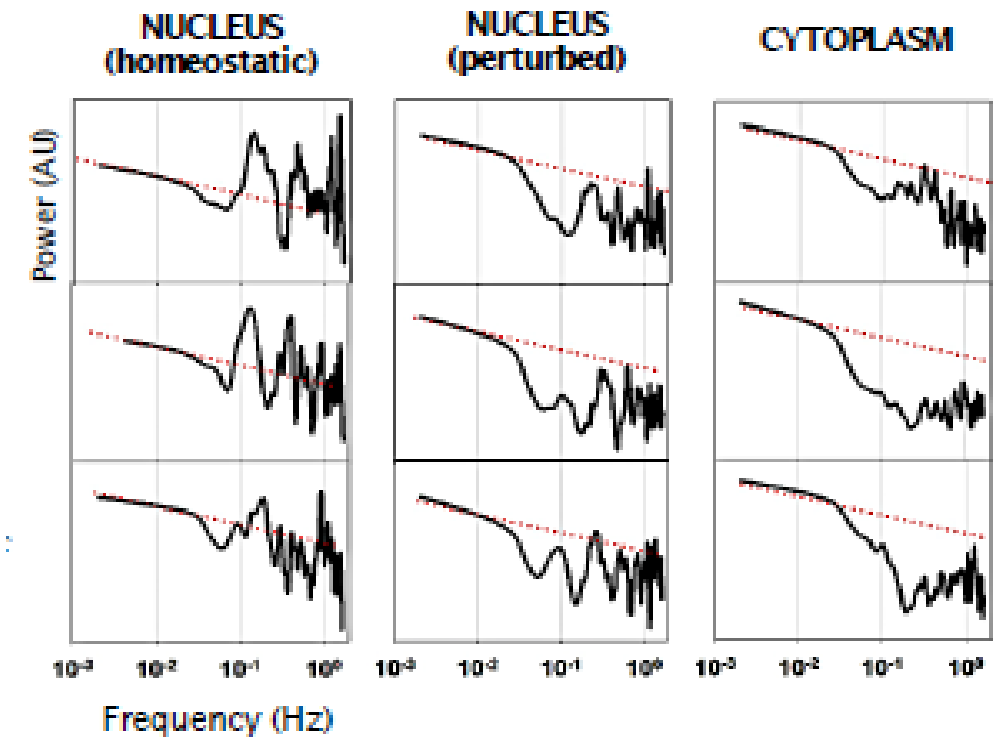

Figure 13 Representative power spectra decompositions in 3 different nuclei at 37°C (first column), following 50% decrease in PBS concentration (second column), & in cytoplasm (third column)

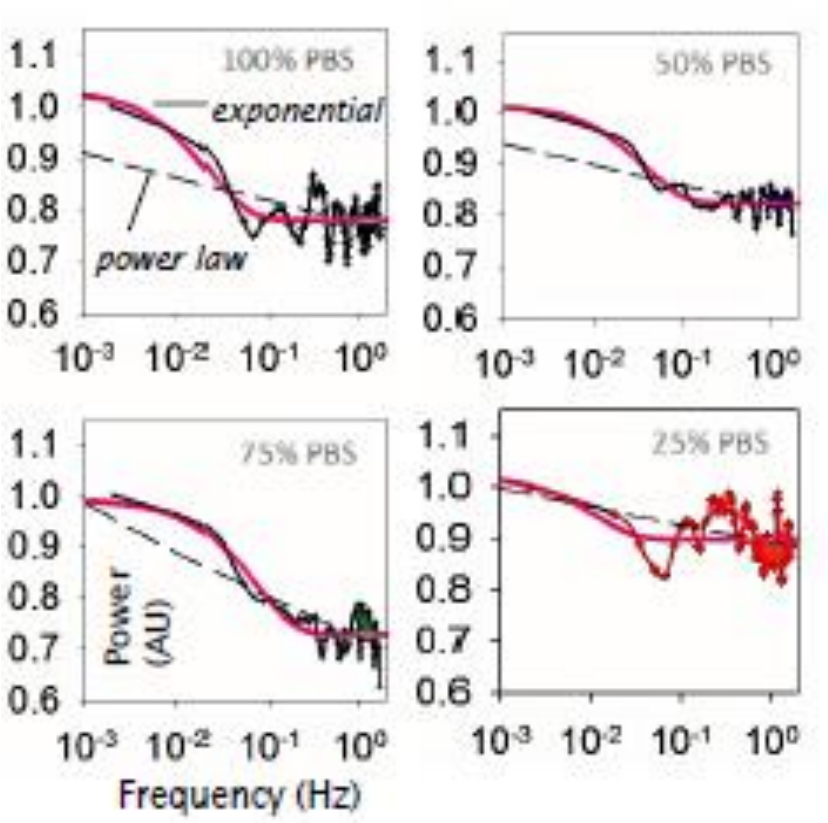

Figure 14 Spectral decomposition of BLS fluctuations for different PBS concentrations. Fluctuations at characteristic frequency are attenuated and high frequency noise increases as PBS concentration decreases, suggesting cells lose ability to suppress noise.

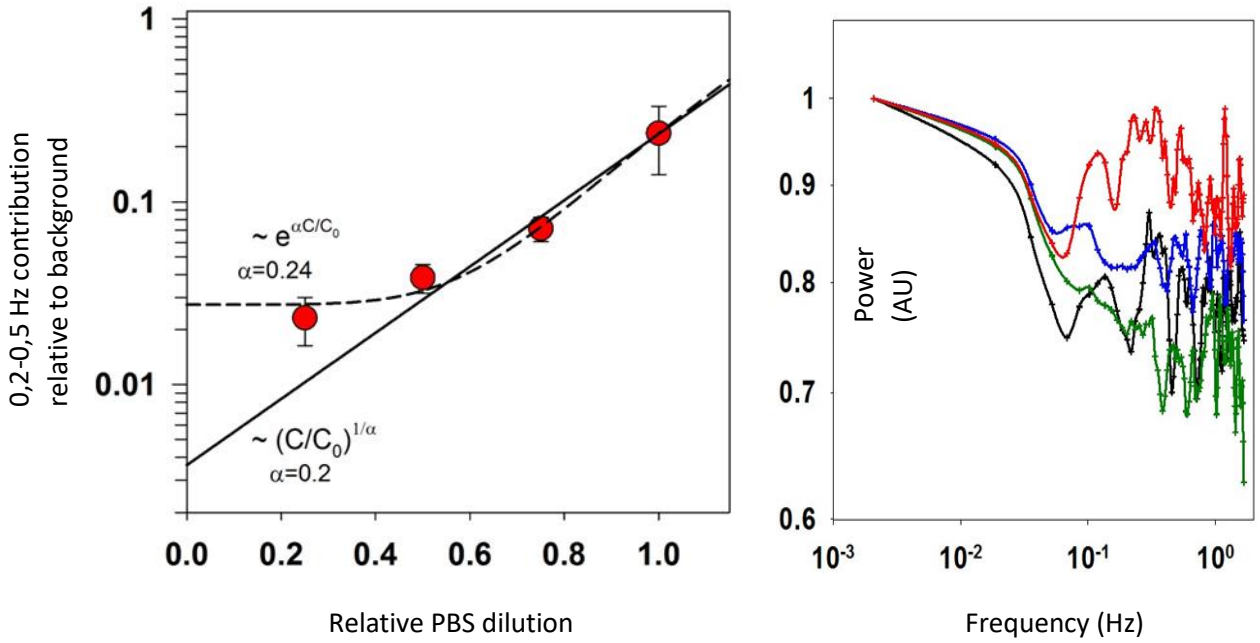

Figure 15 Enhancement of high frequency noise away from homeostatic PBS concentrations (obtained from fitting spectra with exponential function).

Temperature perturbations

We can also investigate the effect of different temperatures on the nuclear state oscillations (*Fig. 16)*. Here we find a suppression of the characteristic frequency oscillations observed at 37°C especially for lower temperatures. Interestingly these are not so affected at slightly elevated temperatures (39°C) but again suppressed at higher temperatures (41°C). To quantify this we can calculate the relative spectra enhancement at 0.3-0.5 Hz relative to the background (fitted by an exponential function) as shown in *Fig. 15*. We find that this is enhanced at 37-39°C, suggesting that away from homeostatic conditions there is a loss of coherence in nuclear fluctuations. *Fig. 17* shows the enhancement of 0.3-0.5Hz contribution relative to high frequency background that can be well fitted by a Lorentzian function which is consistent with this being a resonant phenomenon and expected for a system being perturbed away from a critical state. We can also explicitly plot the background noise for the different temperatures obtained by exponential smoothing of the spectral decomposition (*Fig. 18)*. Here we again see that away from homeostatic conditions (37°C) the white noise is significantly enhanced in the studied spectral range. While the mechanism underlying this is still illusive and requires further theoretical and experimental studies, one may speculate that the coherent oscillations serve to channel the energy from the otherwise incoherent dynamics (presumably from the broad thermal spectra) to create the transient structure in the nucleus that has been previously reported by ourselves as well as others using Displacement Correlation Spectroscopy (DCS) (15,16) and Brillouin Light Scattering Anisotropy Microscopy (31,50).

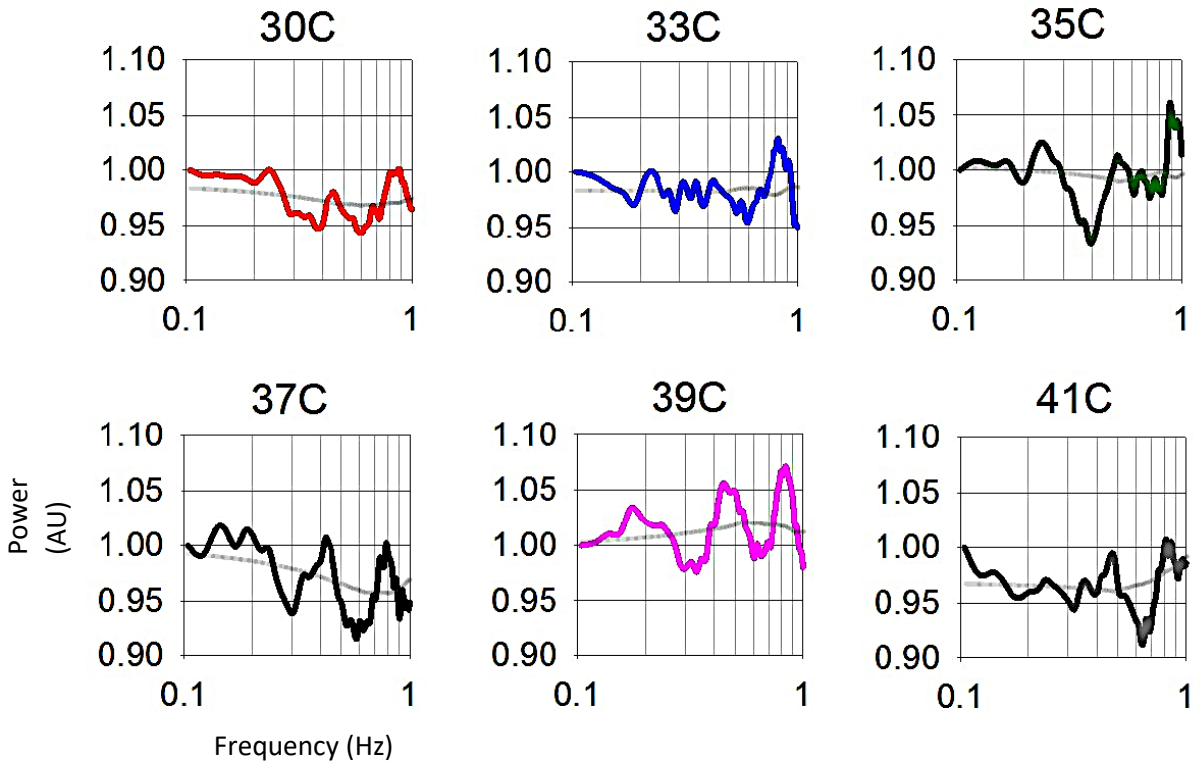

Figure 16 Power spectrum of BLS frequency shift in nuclei at different temperatures. Points represent point measurements in the nucleus, corresponding to different thermodynamic conditions.

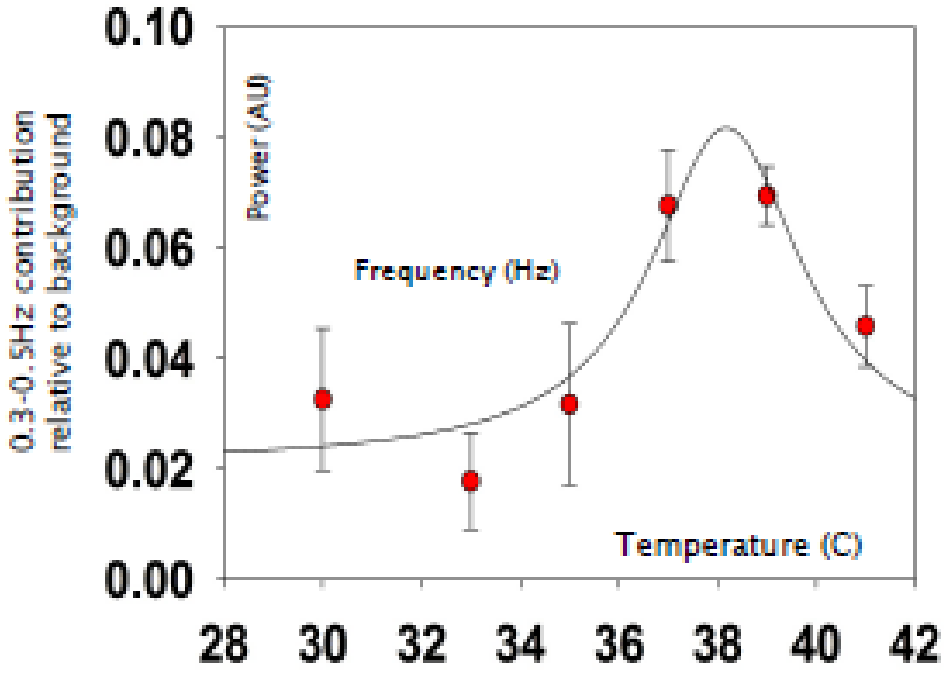

Figure 17 Enhancement of 0.3-0.5Hz contribution relative to high frequency background at different temperatures. Points are measurements in the nucleus and error bars are standard errors.

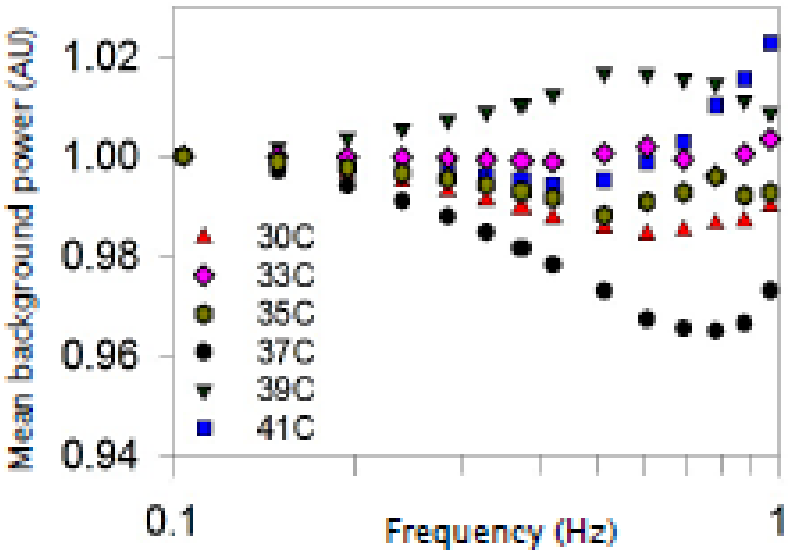

Figure 18 Normalized Background noise of BLS power spectra at different temperatures as function of frequency, showing that noise appears to be suppressed at 37 °C.

3.5. Discussion

A decrease in Brillouin frequency shift fluctuations was observed away from homeostatic conditions (PBS concentrations and 37 °C). This phenomenon could potentially be linked to the existence of the nucleus in the vicinity of a state finely tuned to support resonant-like fluctuations for specific electrostatic environments (ion concentrations) and thermodynamic conditions. This is qualitatively supportive of previous observations and recently proposed models of nuclear dynamics (20). Arguably the most interesting finding here though is how the existence in this homeostatic state also inhibits the noise (see above). This is both surprising and expected. Surprising in the sense that we did not imagine this would be so pronounced/detectable. Expected in the sense that we know many biological processes are very sensitive to the "physical" conditions, and pushing them out of some static or dynamic equilibrium causes all kinds of things to go "haywire" (cease to function in a very drastic way). While this project has focused very much on the experimental challenges, it would be interesting to look into the temporal dynamics from an information theoretical perspective, and the produced results may lead to some much deeper interpretations on how the nucleus functions in an ordered way (despite being a messy polymer soup). However this extension is a project more suited for a theoretical physicist (rather than an experimental biologist) and we hope that they will be able use the extensive data I have generated to give us a deeper insight

into what makes the nucleus function so efficiently, change so dynamically, and maybe even some fundamental insight into what makes a living system alive!

3.6. Conclusion and importance of results

Through Brillouin spectroscopy analysis, we have gained an understanding of ionic concentration and temperature perturbation experiments on the 0.1-1 Hz nuclear picosecond mechanical oscillations. These findings are in alignment with predictions derived from a straightforward reaction-diffusion model. Furthermore, our results indicate that the nucleus utilizes these coherent mechanical oscillations effectively to counteract (thermal) noise and establish transient structural stability. This transient structure potentially plays a role in dynamic intranuclear mechanical signalling. We are planning additional experiments involving specific molecular perturbations, such as different cation species and proteins known to actively or passively influence chromatin state. Additionally, localized thermodynamic perturbations are under consideration to further refine our model.

Our goal is to pinpoint the various molecular and thermodynamic parameters necessary for dynamic nuclear mechanical properties to closely resemble those observed under homeostatic conditions. Achieving this goal holds significant potential in offering crucial insights into the underlying mechanisms of various diseases where these properties are perturbed. Moreover, such insights can shed light on strategies for corrective interventions.

Chapter 4: General conclusions, outlook and future perspectives.

In this thesis we present the application of Brillouin Light Scattering (BLS) spectroscopy to study two very different systems with very different aims. In the first section, we delve into the application of Brillouin Light Scattering (BLS) for assessing the mechanical properties of various parts of the human anatomy, including veins, arteries, nerves, and muscles. This exploration serves a dual purpose. Firstly, it aims to provide insights into the distinct mechanical properties of these tissues, potentially shedding light on their functional and biophysical aspects. Secondly, it acknowledges that alterations in the mechanics of these

tissues are often associated with the onset of various diseases. Cataloging the properties of these tissues in their non-diseased state represents a crucial initial step in detecting changes in diseased tissues.

BLS offers a label-free, all-optical method for measuring these properties, holding significant potential for future clinical applications. However, previous implementations have necessitated bulky microscopy setups, making them unsuitable for clinical translation. To address this issue, we have designed and developed an optical handheld probe for BLS measurements, intended for use by clinicians. We have also tested its performance in comparison to the cumbersome laboratory setup for distinguishing various excised tissues.

The design of the probe required careful consideration of several important parameters to ensure its robustness, reliability, and ease of use. These parameters, discussed in more detail in the thesis, include simultaneous measurements from multiple points in a sample to obtain an effective or average value for heterogeneous tissue, high coupling efficiency to minimize laser energy exposure to the tissue, and low numerical aperture probing and detecting optics to minimize broadening of the BLS peaks measured. Another crucial feature involved on-the-fly spectral registration using a control sample mounted in the probe, allowing for rapid and routine calibration to ensure high-precision measurements immediately following a straightforward internal calibration.

Our results reveal distinct elastic and viscous moduli for the various tissues studied, as shown in Table 1. These results can be reliably reproduced within experimental certainty using the bulky laboratory setup (see *Figure 5A*). We observe interesting trends, such as arteries consistently displaying higher moduli than veins (see *Figure 5 B-D*), and a gradual yet significant change in modulus within the same veins further up the arm (see *Figure 6A-E*). Some of these trends have been reported in previous quasi-static tensile and shear measurements. We attempt to explain our observations in the context of the measured modulus, which is obtained under distinct boundary conditions and at significantly higher frequencies than the quasi-static modulus often measured. In particular, we demonstrate how changes in the characteristic viscous relaxation time can qualitatively account for the observed behavior (see *Figure 6 C and E*).

Our results represent a vital first step towards the clinical implementation of BLS by introducing a device suitable for performing assessments directly on various parts of the human body. This device can be easily operated by medical professionals. Future efforts will focus on characterizing different tissues in the hope of establishing a comprehensive BLS

atlas, cataloging standard physiological values of elastic and viscous moduli for different tissues. Once measurement protocols and such a database are established, investigations into how and if these values are perturbed in pathological tissues can be pursued for potential prognostic and diagnostic applications.

The second section of this thesis shifts its focus to the dynamic mechanical properties of the cell nucleus. While previous studies have primarily examined the static mechanical properties of the nucleus, studying its dynamics is challenging yet crucial for understanding nuclear processes and their responses to various chemical and environmental changes. BLS operates in a unique regime, probing very short time scales where even liquids exhibit solid-like behavior. This sensitivity to transient structures on these time scales, such as those associated with crosslinking or short-lived hydrodynamic interactions between solutes/suspensions and solvents, becomes especially relevant given that the nucleus comprises approximately 70% of the cell.

Recent observations by our research group and others suggest that chromatin itself is highly dynamic, with characteristic fluctuations occurring on the order of several seconds, closely tied to chromatin state and structure. Considering BLS's sensitivity to chromatin state, we investigate whether these fluctuations can be observed using BLS. Our findings confirm the presence of such fluctuations in living HeLa cells, with power spectrum analysis revealing enhanced oscillations in the range of 0.1-0.2 Hz (see *Figures 13-18*).

To test a recently proposed model that predicts these fluctuations' sensitivity to the electrostatic landscape and thermodynamic conditions, we systematically perturb the cells (see *Figure 9*). Firstly, we dilute their buffer, effectively reducing the cation concentration, which the nucleus can be assumed to be permeable to. This perturbation noticeably compromises the power spectra, leading to reduced oscillations (see *Figures 13-15*). Another perturbation involves altering the temperature, where we observe that the optimal temperature for oscillations is 37°C, suggesting that the observed oscillations are a result of the nucleus existing in a delicate equilibrium(see *Figures 16-18*). Additionally, we notice that the residual noise in the power spectrum is significantly attenuated at optimal PBS concentrations and around 37°C (see *Figures 15 and 18*). We are currently working on understanding the theoretical basis for this phenomenon and its physiological relevance.

To gain a deeper understanding of these observations, further experiments are needed. These include systematically varying the concentration of specific ions/cations and molecular species known to inhibit/promote chromatin condensation and perturbing different active

nuclear processes. Additionally, examining the spatial and temporal scales of these fluctuations and their behavior during different cell cycles (our studies focused on interphase cells) would be intriguing.

Our observations in this section mark a significant first step in confirming the existence of dynamic mechanical changes in the nucleus and demonstrate the feasibility of studying them using BLS.

In summary, this thesis showcases the versatility of BLS in two distinct applications: studying macroscopic mechanical changes in tissue and dynamic microscopic nuclear processes. Advancements in both areas are anticipated to align with improvements in technology, such as better spectrometers and handheld probes, and will benefit from comprehensive correlative studies and investigations under different perturbations. The research presented here represents critical progress in these respective directions.

References

(n.d.).

1. Antonacci, G., Beck, T., Bilenca, A., Czarske, J., Elsayad, K., Guck, J., Kim, K., Krug, B., Palombo, F., Prevedel, R., & Scarcelli, G. (2020). Recent progress and current opinions in Brillouin microscopy for life science applications. *Biophysical Reviews*, *12*(3), 615–624. https://doi.org/10.1007/s12551-020-00701-9
2. Antonacci, G., & Braakman, S. (2016). Biomechanics of subcellular structures by non-invasive Brillouin microscopy. *Scientific Reports*, *6*, 37217. https://doi.org/10.1038/srep37217
3. Bailey, M., Alunni-Cardinali, M., Correa, N., Caponi, S., Holsgrove, T., Barr, H., Stone, N., Winlove, C. P., Fioretto, D., & Palombo, F. (2020). Viscoelastic properties of biopolymer hydrogels determined by Brillouin spectroscopy: A probe of tissue micromechanics. *Science Advances*, *6*(44). https://doi.org/10.1126/sciadv.abc1937
4. Belmont, A. S. (2001). Visualizing chromosome dynamics with GFP. *Trends in Cell Biology*, *11*(6), 250–257. https://doi.org/10.1016/s0962-8924(01)02000-1
5. Berovic, N., Thomas, N., Thornhill, R. A., & Vaughan, J. M. (1989). Observation of Brillouin scattering from single muscle fibres. *European Biophysics Journal : EBJ*, *17*(2), 69–74. https://doi.org/10.1007/BF00257104
6. Brandon Ward. (2019). *How to Measure the Size of a Specimen Under the Microscope*. Microscope Clarity.

7. Bruinsma, R., Grosberg, A. Y., Rabin, Y., & Zidovska, A. (2014). Chromatin hydrodynamics. *Biophysical Journal*, *106*(9), 1871–1881. https://doi.org/10.1016/j.bpj.2014.03.038
8. Chubb, J. R., & Bickmore, W. A. (2003). Considering nuclear compartmentalization in the light of nuclear dynamics. *Cell*, *112*(4), 403–406. https://doi.org/10.1016/s0092-8674(03)00078-3
9. Courtney, T. H. (1990). *Mechanical behavior of materials*. McGraw-Hill.
10. Croft, J. A., Bridger, J. M., Boyle, S., Perry, P., Teague, P., & Bickmore, W. A. (1999). Differences in the localization and morphology of chromosomes in the human nucleus. *The Journal of Cell Biology*, *145*(6), 1119–1131. https://doi.org/10.1083/jcb.145.6.1119
11. Dowdell, J., Kim, J., Overley, S., & Hecht, A. (2018). Biomechanics and common mechanisms of injury of the cervical spine. *Handbook of Clinical Neurology*, *158*, 337–344. https://doi.org/10.1016/B978-0-444-63954-7.00031-8
12. Drieskens, L., Fevery, J., & de Groote, J. (1972). [Malignant tumors of the liver]. *Tijdschrift Voor Gastro-Enterologie*, *15*(5), 346–370.
13. Egan, P., Sinko, R., LeDuc, P. R., & Keten, S. (2015). The role of mechanics in biological and bio-inspired systems. *Nature Communications*, *6*, 7418. https://doi.org/10.1038/ncomms8418
14. Ellenberg, J., & Lippincott-Schwartz, J. (1999). Dynamics and mobility of nuclear envelope proteins in interphase and mitotic cells revealed by green fluorescent protein chimeras. *Methods (San Diego, Calif.)*, *19*(3), 362–372. https://doi.org/10.1006/meth.1999.0872
15. Elsayad, K., Palombo, F., Dehoux, T., & Fioretto, D. (2019). Brillouin Light Scattering Microspectroscopy for Biomedical Research and Applications: introduction to feature issue. *Biomedical Optics Express*, *10*(5), 2670–2673. https://doi.org/10.1364/BOE.10.002670
16. Fiore, A., Zhang, J., Shao, P., Yun, S. H., & Scarcelli, G. (2016). High-extinction virtually imaged phased array-based Brillouin spectroscopy of turbid biological media. *Applied Physics Letters*, *108*(20), 203701. https://doi.org/10.1063/1.4948353
17. Hamid Keshmiri, D. C. M. S. L. S. L.-M. A. M. U. I. Y. D. S. W. J. W. A. P. J. P. K. E. (2023). Imaging the microscopic viscoelastic anisotropy in living cells. *BioRxiv*.
18. Hytowitz, A. N. (2023). Review of using the Dyop optotype for acuity and refractions per the article: https://www.sciencedirect.com/science/article/pii/S1888429622000656. *Journal of Optometry*. https://doi.org/10.1016/j.optom.2022.12.002
19. Karduna, A. R. (2012). Understanding the biomechanical nature of musculoskeletal tissue. *Journal of Hand Therapy : Official Journal of the American Society of Hand Therapists*, *25*(2), 116–121; quiz 122. https://doi.org/10.1016/j.jht.2011.12.006
20. Klaus Suhling, J. S. †, D. P., P. M. W. F. †, S. L.-F. , S. E. D. W. , D. M. D. . (2002). Imaging the Environment of Green Fluorescent Protein. *Biophysical Journal*, *83*(6), 3589–3595.
21. Koski, K. J., Akhenblit, P., McKiernan, K., & Yarger, J. L. (2013). Non-invasive determination of the complete elastic moduli of spider silks. *Nature Materials*, *12*(3), 262–267. https://doi.org/10.1038/nmat3549

22. Laghmach, R., Di Pierro, M., & Potoyan, D. (2022). A Liquid State Perspective on Dynamics of Chromatin Compartments. *Frontiers in Molecular Biosciences*, *8*. https://doi.org/10.3389/fmolb.2021.781981
23. Landge, A. N., Jordan, B. M., Diego, X., & Müller, P. (2020). Pattern formation mechanisms of self-organizing reaction-diffusion systems. *Developmental Biology*, *460*(1), 2–11. https://doi.org/10.1016/j.ydbio.2019.10.031
24. Lebeaupin, T., Smith, R., & Huet, S. (2017). The Multiple Effects of Molecular Crowding in the Cell Nucleus. In *Nuclear Architecture and Dynamics* (pp. 209–232). Elsevier. https://doi.org/10.1016/B978-0-12-803480-4.00009-0
25. Lee, D. S. W. , W. N. S. & B. C. P. (2020). Chromatin mechanics dictates subdiffusion and coarsening dynamics of embedded condensates. *Nat. Phys*, *18*, 531–538.
26. Lee, S. A., Lindsay, S. M., Powell, J. W., Weidlich, T., Tao, N. J., & Lewen, G. D. (1987a). A Brillouin scattering study of the hydration of Li- and Na-DNA films. *Biopolymers*, *26*(10), 1637–1665. https://doi.org/10.1002/bip.360261002
27. Lee, S. A., Lindsay, S. M., Powell, J. W., Weidlich, T., Tao, N. J., & Lewen, G. D. (1987b). A Brillouin scattering study of the hydration of Li- and Na-DNA films. *Biopolymers*, *26*(10), 1637–1665. https://doi.org/10.1002/bip.360261002
28. Lippincott-Schwartz, J., & Patterson, G. H. (2003). Development and use of fluorescent protein markers in living cells. *Science (New York, N.Y.)*, *300*(5616), 87–91. https://doi.org/10.1126/science.1082520
29. Liu, B., Poolman, B., & Boersma, A. J. (2017). Ionic Strength Sensing in Living Cells. *ACS Chemical Biology*, *12*(10), 2510–2514. https://doi.org/10.1021/acschembio.7b00348
30. Maria-Elena Torres-Padilla. (2013, October 7). *Gene movements observed in vivo*.
31. Meng, Z., Bustamante Lopez, S. C., Meissner, K. E., & Yakovlev, V. V. (2016). Subcellular measurements of mechanical and chemical properties using dual Raman-Brillouin microspectroscopy. *Journal of Biophotonics*, *9*(3), 201–207. https://doi.org/10.1002/jbio.201500163
32. Menon, G. I. (2020). Chromatin as an active polymeric material. *Emerging Topics in Life Sciences*, *4*(2), 111–118. https://doi.org/10.1042/ETLS20200010
33. Miller, R. C., Aplin, C. P., Kay, T. M., Leighton, R., Libal, C., Simonet, R., Cembran, A., Heikal, A. A., Boersma, A. J., & Sheets, E. D. (2020). FRET Analysis of Ionic Strength Sensors in the Hofmeister Series of Salt Solutions Using Fluorescence Lifetime Measurements. *The Journal of Physical Chemistry. B*, *124*(17), 3447–3458. https://doi.org/10.1021/acs.jpcb.9b10498
34. Misteli, T. (2004). Spatial positioning; a new dimension in genome function. *Cell*, *119*(2), 153–156. https://doi.org/10.1016/j.cell.2004.09.035
35. Misteli, T. (2007). Beyond the sequence: cellular organization of genome function. *Cell*, *128*(4), 787–800. https://doi.org/10.1016/j.cell.2007.01.028
36. Palombo, F., & Fioretto, D. (2019). Brillouin Light Scattering: Applications in Biomedical Sciences. *Chemical Reviews*, *119*(13), 7833–7847. https://doi.org/10.1021/acs.chemrev.9b00019
37. Paoletti, E. (1990). Poxvirus recombinant vaccines. *Annals of the New York Academy of Sciences*, *590*, 309–325. https://doi.org/10.1111/j.1749-6632.1990.tb42239.x

38. Pederson, T., King, M. C., & Marko, J. F. (2015a). Forces, fluctuations, and self-organization in the nucleus. *Molecular Biology of the Cell*, *26*(22), 3915–3919. https://doi.org/10.1091/mbc.E15-06-0357
39. Pederson, T., King, M. C., & Marko, J. F. (2015b). Forces, fluctuations, and self-organization in the nucleus. *Molecular Biology of the Cell*, *26*(22), 3915–3919. https://doi.org/10.1091/mbc.E15-06-0357
40. Prevedel, R., Diz-Muñoz, A., Ruocco, G., & Antonacci, G. (2019). Brillouin microscopy: an emerging tool for mechanobiology. *Nature Methods*, *16*(10), 969–977. https://doi.org/10.1038/s41592-019-0543-3
41. Pruidze, P., Chayleva, E., Weninger, W. J., & Elsayad, K. (2023). Brillouin scattering spectroscopy for studying human anatomy: Towards *in situ* mechanical characterization of soft tissue. *Journal of the European Optical Society-Rapid Publications*, *19*(1), 31. https://doi.org/10.1051/jeos/2023028
42. Ravi Theja V. Chintapalli and Julián F. Hillyer*. (2016). Hemolymph circulation in insect flight appendages: physiology of the wing heart and circulatory flow in the wings of the mosquito Anopheles gambiae. *Journal of Experimental Biology*, *219*(24), 3945–3951.
43. Ross Ethier, C., & Simmons, C. A. (n.d.). *Introductory Biomechanics: From Cells to Organisms*.
44. Ryu, S., Martino, N., Kwok, S. J. J., Bernstein, L., & Yun, S.-H. (2021a). Label-free histological imaging of tissues using Brillouin light scattering contrast. *Biomedical Optics Express*, *12*(3), 1437–1448. https://doi.org/10.1364/BOE.414474
45. Ryu, S., Martino, N., Kwok, S. J. J., Bernstein, L., & Yun, S.-H. (2021b). Label-free histological imaging of tissues using Brillouin light scattering contrast. *Biomedical Optics Express*, *12*(3), 1437–1448. https://doi.org/10.1364/BOE.414474
46. Salcedo, M. K., Jun, B. H., Socha, J. J., Pierce, N. E., Vlachos, P. P., & Combes, S. A. (2023). Complex hemolymph circulation patterns in grasshopper wings. *Communications Biology*, *6*(1), 313. https://doi.org/10.1038/s42003-023-04651-2
47. Satija, S. K., & Wang, C. H. (1978). Brillouin scattering study of elastic anomaly in (KCN)x(KBr)1−x system. *Solid State Communications*, *28*(8), 617–619. https://doi.org/10.1016/0038-1098(78)90592-6
48. Scarcelli, G., Besner, S., Pineda, R., & Yun, S. H. (2014). Biomechanical characterization of keratoconus corneas ex vivo with Brillouin microscopy. *Investigative Ophthalmology & Visual Science*, *55*(7), 4490–4495. https://doi.org/10.1167/iovs.14-14450
49. Scarcelli, G., Pineda, R., & Yun, S. H. (2012). Brillouin optical microscopy for corneal biomechanics. *Investigative Ophthalmology & Visual Science*, *53*(1), 185–190. https://doi.org/10.1167/iovs.11-8281
50. Scarcelli, G., Polacheck, W. J., Nia, H. T., Patel, K., Grodzinsky, A. J., Kamm, R. D., & Yun, S. H. (2015). Noncontact three-dimensional mapping of intracellular hydromechanical properties by Brillouin microscopy. *Nature Methods*, *12*(12), 1132–1134. https://doi.org/10.1038/nmeth.3616
51. Schneck, D. J., & Bronzino, J. D. (2003). *Biomechanics : principles and applications*. CRC Press.
52. Siddharth Neog, V. T. (2022). *Approaches and methods to study cell signaling: Linguistics of cellular communication*.

53. Soboleski, M. R., Oaks, J., & Halford, W. P. (2005). Green fluorescent protein is a quantitative reporter of gene expression in individual eukaryotic cells. *FASEB Journal : Official Publication of the Federation of American Societies for Experimental Biology*, *19*(3), 440–442. https://doi.org/10.1096/fj.04-3180fje
54. Stephens, A. D., Banigan, E. J., & Marko, J. F. (2019). Chromatin's physical properties shape the nucleus and its functions. *Current Opinion in Cell Biology*, *58*, 76–84. https://doi.org/10.1016/j.ceb.2019.02.006
55. Tessa N. Campbell and Francis Y.M. Choy. (2001). The Effect of pH on Green Fluorescent Protein: a Brief Review. *Caister Academic Press*, *2*(1), 1–4.
56. Théo Lebeaupin 1 2, R. S. 3, S. H. 1 2. (2018). The Multiple Effects of Molecular Crowding in the Cell Nucleus: From Molecular Dynamics to the Regulation of Nuclear Architecture. *Nuclear Architecture and Dynamics*, 209–232.
57. Traverso, A. J., Thompson, J. V, Steelman, Z. A., Meng, Z., Scully, M. O., & Yakovlev, V. V. (2015). Dual Raman-Brillouin Microscope for Chemical and Mechanical Characterization and Imaging. *Analytical Chemistry*, *87*(15), 7519–7523. https://doi.org/10.1021/acs.analchem.5b02104
58. Vaughan, J. M., & Randall, J. T. (1980). Brillouin scattering, density and elastic properties of the lens and cornea of the eye. *Nature*, *284*(5755), 489–491. https://doi.org/10.1038/284489a0
59. Villena Gonzales, W., Mobashsher, A. T., & Abbosh, A. (2019). The Progress of Glucose Monitoring-A Review of Invasive to Minimally and Non-Invasive Techniques, Devices and Sensors. *Sensors (Basel, Switzerland)*, *19*(4). https://doi.org/10.3390/s19040800
60. World Health Organisation. (2020). *The top 10 causes of death*.
61. Zhang, G., Gurtu, V., & Kain, S. R. (1996). An enhanced green fluorescent protein allows sensitive detection of gene transfer in mammalian cells. *Biochemical and Biophysical Research Communications*, *227*(3), 707–711. https://doi.org/10.1006/bbrc.1996.1573
62. Zhang, J., Alisafaei, F., Nikolić, M., Nou, X. A., Kim, H., Shenoy, V. B., & Scarcelli, G. (2020). Nuclear Mechanics within Intact Cells Is Regulated by Cytoskeletal Network and Internal Nanostructures. *Small*, *16*(18). https://doi.org/10.1002/smll.201907688
63. Zidovska, A. (2020). The rich inner life of the cell nucleus: dynamic organization, active flows, and emergent rheology. *Biophysical Reviews*, *12*(5), 1093–1106. https://doi.org/10.1007/s12551-020-00761-x
64. Zidovska, A. (2021). Nuclear espionage. In *Nature Physics* (Vol. 17, Issue 4, pp. 436–437). Nature Research. https://doi.org/10.1038/s41567-020-01133-8
65. Zidovska, A., Weitz, D. A., & Mitchison, T. J. (2013). Micron-scale coherence in interphase chromatin dynamics. *Proceedings of the National Academy of Sciences of the United States of America*, *110*(39), 15555–15560. https://doi.org/10.1073/pnas.1220313110